Driving proteomic imbalance to combat Neurofibromatosis type I (NF1)-associated malignancy

Babul Moni Ram[1], Kun-Han Chuang[1,2], and Chengkai Dai[1,*]

[1]Mouse Cancer Genetics Program, Center for Cancer Research, National Cancer Institute, Frederick, MD 21702, USA

[2]Present address: School of Basic Medical Sciences, Fujian Medical University, Fuzhou, Fujian 350108, China

*Correspondence: Chengkai.dai@nih.gov

ABSTRACT

Unlike genomic instability, the implications of proteomic instability in cancer remain ambiguous. By governing the proteotoxic stress response, heat shock factor 1 (HSF1) sustains proteomic stability upon environmental insults. Apart from its importance to stress resistance and survival, HSF1 is emerging as a powerful, generic oncogenic enabler. In the Neurofibromatosis type I (*NF1*)-deficient malignant peripheral nerve sheath tumor (MPNST) cells, *HSF1* depletion prompted protein polyubiquitination, aggregation, and even tumor-suppressive amyloidogenesis. In stark contrast, *HSF1* is dispensable for the proteome of non-transformed human Schwann cells. Mechanistically, in MPNST cells HSF1 defends the essential mitochondrial chaperone HSP60 against the direct assault from soluble amyloid oligomers. To survive and adapt to impaired protein quality, owing to *HSF1* deficiency, MPNST cells mobilized JNK to repress mTORC1 and protein translation, thereby attenuating protein quantity to alleviate proteomic imbalance. mTORC1 stimulation, via either pharmacological JNK blockade, genetic *TSC2* depletion, or supplement with the leucine analog NV-5138, markedly aggravated the proteomic imbalance elicited by *HSF1* deficiency. This profound proteomic imbalance instigated non-apoptotic cell death partly through unchecked amyloidogenesis. Thus, HSF1 safeguards the cancer proteome to enable the oncogenic potential of mTORC1. Counterintuitively, this proof-of-concept study highlights driving proteomic imbalance as a new therapeutic concept to combat malignancies.

INTRODUCTION

Compared to genomic instability, proteomic instability in cancer is much less appreciated. Malignant transformation provokes proteotoxic stress and destabilizes the proteome.[1, 2] Several mechanisms, including reactive oxygen species, genetic mutations, and uncontrolled protein translation, all lead to increased protein damage, misfolding, as well as aggregation.[1-3] Of great interest, amyloidogenesis, a hallmark of neurodegenerative disorders,[4] also occurs in cancer.[5] Unlike neurons, cancerous cells manage to contain amyloidogenesis and counteract the cytotoxic effects of amyloids. Among various cellular anti-amyloid mechanisms is heat shock factor 1 (HSF1) and its mediated heat shock response or proteotoxic stress response (HSR/PSR), a powerful cytoprotective transcriptional program.[6-8] In accordance with its role in repressing proteomic instability, HSF1 has emerged as a potent oncogenic enabler, independently of driver mutations.[9-15]

Sharply contrasting with its dispensability for primary and non-transformed cells, HSF1 becomes essential to numerous cancer cell lines,[9,13,16-18] owing to their elevated intrinsic proteotoxic stress. This phenomenon is referred to as "HSF1 or non-oncogene addiction of cancer",[2,19] justifying HSF1 as a promising therapeutic target.

Neurofibromatosis type 1 (NF1) is a cancer predisposition syndrome afflicting approximately 1 in 3000 individuals worldwide.[20] About 30-50% of NF1 individuals develop benign plexiform neurofibromas, which, unlike dermal neurofibromas, can transform into highly aggressive malignant peripheral nerve sheath tumors (MPNSTs) with poor prognosis and survival.[21] The *NF1* gene encodes neurofibromin, a 250-280 kDa RAS GTPase activating protein (GAP) that

negatively regulates RAS activity.[22] *NF1* inactivation in MPNST cells dysregulates RAS/MAPK signaling which, in addition to stimulating cell growth, leads to constitutive HSF1 activation.[13] Concomitantly, HSF1 overexpression and activation are seen in both *in vitro* and *in vivo* MPNST models as well as primary NF1 tumors.[13] Importantly, *Hsf1* deficiency impaired the NF1-associated tumorigenesis in mice in part by attenuating oncogenic RAS signaling.[13]

Utilizing the NF1 tumor model system, we herein demonstrate HSF1 as a key player in countering proteomic instability in cancer. We discover that amyloidogenesis occurs in *NF1*-deficient MPNST cells, partly due to hyperactive mTORC1 and augmented protein translation. HSF1 inhibition destabilizes the cancer proteome, promoting global protein polyubiquitination, aggregation, as well as amyloidogenesis. Importantly, this proteomic instability causes cytotoxicity. To adapt and survive HSF1 inhibition, MPNST cells mobilize JNK to suppress mTORC1 and thereby mitigate protein translation. Disrupting this adaptative response through JNK inhibition aggravates amyloidogenesis and cytotoxicity. Similarly, mTORC1 stimulation, via either genetic *TSC2* depletion or supplement with the leucine analog NV-5138, synergizes with HSF1 inhibition to inflict profound proteomic chaos and widespread non-apoptotic cell death. Of note, impairment of amyloidogenesis markedly blocks cell death. Thus, our findings illuminate a prominent role of HSF1 in antagonizing proteomic instability in cancerous cells, constituting a generic pro-oncogenic mechanism. Moreover, this study exemplifies a proof of concept that highlights driving proteomic imbalance as a counterintuitive therapeutic strategy.

RESULTS

HSF1 counters proteomic instability in *NF1*-deficient MPNST cells

Previously, we found that loss of *NF1* leads to constitutive activation of HSF1 and that *Hsf1* deficiency impairs the tumorigenesis in *Nf1*$^{+/-}$; *p53*$^{+/-}$ (NPcis) mice.[13] In human cancers, *NF1* deletion is associated with elevated *HSF1* gene expression (Figure 1A). Moreover, the expression of *NF1* and *HSF1* genes are inversely correlated in human cancers (Figure S1A). Importantly, among patients whose tumors harbor *NF1* deletion higher *HSF1* expression is correlated with shortened survival (Figure 1B). Collectively, these findings support a pro-oncogenic role of HSF1 in *NF1*-deficient malignancies.

Given its critical role in governing protein folding, we were curious about how *HSF1* depletion impacts the proteomes of *NF1*-deficient MPNST cells as well as *NF1*-proficient non-transformed human Schwann cells (HSCs), both primary and immortalized. HSCs are considered as the cell-of-origin of MPNSTs.[20,22] In three different MPNST cell lines (90-8TL, S462, and SNF96.2), transient depletion of *HSF1*, using two previously validated lentiviral shRNAs,[9,13] all caused an increase in global protein Lys48-specific polyubiquitination, a molecular mark for proteasomal degradation,[23] in both detergent-soluble and -insoluble fractions (Figures 1C, 1D, S1B, and S1C). This increased polyubiquitination signifies proteome-wide misfolding and aggregation. In stark contrast, this change was not observed in HSCs (Figures 1C and 1D). Thus, *HSF1* depletion provokes proteomic instability in MPNST cells, but not in HSCs.

Most cellular protein aggregates are amorphous; however, a tiny fraction becomes highly ordered and enriched with β-sheet structures. These special protein aggregates, namely amyloids, are

closely associated with neurodegenerative disorders in humans, especially Alzheimer's disease.[24] To assess whether *HSF1* depletion could elicit amyloidogenesis, we stained both MPNST cells and HSCs with Congo red (CR), a widely applied amyloid-binding fluorescent dye.[25] Compared to HSCs, MPNST cells displayed more intense CR staining (Figure 1E), suggesting increased amyloids in malignant Schwann cells. Importantly, *HSF1* depletion further intensified CR staining in MPNST cells, but not in HSCs (Figures 1E, 1F, S1D, and S1E). Similar results were obtained by Thioflavin T staining (Figure S1F), another popular amyloid dye.[25] Importantly, the induction of amyloids was further confirmed by ELISA using two conformation-specific antibodies (A11 and OC), which recognize soluble amyloid oligomers (AOs) and insoluble amyloid fibrils (AFs), respectively.[26,27] Upon *HSF1* depletion, all three MPNST cell lines displayed elevated levels of $A11^+$ AOs and OC^+ AFs (Figures 1G, 1H, S1G-S1J). Again, no evident increase in amyloids was detected in HSCs (Figures 1I and 1J). Together, these findings indicate that HSF1 is required to safeguard the proteome of malignant Schwann cells and particularly to repress amyloidogenesis; on the contrary, it is dispensable for the proteome of non-transformed Schwann cells.

Unchecked proteomic instability is tumor suppressive

It has become evident that HSF1 acts as a generic oncogenic enabler; nevertheless, a universal underlying mechanism remains undefined.

A healthy proteome enables the translation of genotypes into phenotypes. Thus, we reasoned that preservation of proteomic stability is most likely a generic pro-oncogenic mechanism of HSF1. To test this notion, we first determined whether proteomic instability, particularly amyloidogenesis, is causally related to the cytotoxicity induced by *HSF1* depletion in cancer

139 cells. To block amyloidogenesis we employed CR, which is known to exert anti-amyloid effects
140 through its amyloid-binding activity.[5,28,29] Consistent with "HSF1 addiction of cancer", *HSF1*
141 depletion markedly impaired the viability of MPNST cells; importantly, CR treatment partially
142 rescued this impaired viability (Figures 2A, S2A, and S2B). In contrast, both *HSF1* depletion and
143 CR treatment did not affect HSCs (Figure 2B), congruent with a lack of proteomic instability and
144 amyloidogenesis in these non-transformed cells. Together, these findings support that unchecked
145 proteomic instability, particularly amyloidogenesis, is cytotoxic and tumor suppressive.
146 Moreover, HSF1 enables oncogenesis in part by constraining proteomic instability.
147

148 **HSF1 neutralizes soluble amyloid oligomers to protect MPNST cells**

149 Then, how does HSF1 counter amyloids to enable the growth and survival of MPNST cells?
150 Recently, by researching tissue overgrowth models we discovered that HSF1, surprisingly,
151 physically neutralizes soluble AOs, thereby preventing their assault on HSP60.[30] As an essential
152 mitochondrial chaperone, HSP60 functions as a guardian of the mitochondrial proteome.[30-32]
153

154 We wondered whether HSF1 acts the same way in both cancer and tissue overgrowth. Co-IP
155 experiments indicated that $A11^+$ AOs physically interacted with HSF1, but not major HSPs, in
156 MPNST cells (Figure 2C), consistent with our findings in tissue overgrowth models.[30] This AO-
157 HSF1 interaction was further validated by another independent technique, *in situ* Proximity
158 Ligation Assay (PLA) (Figures 2D-2F). Importantly, *HSF1* depletion promoted the AO-HSP60
159 interaction (Figure 2G and 2H). Loss of *HSP60* destabilized the mitochondrial proteome.[30,32]
160 Thus, this AO-HSP60 interaction signifies the instigation of mitochondrial damage and

161 cytotoxicity. Taken together, our findings reveal that HSF1 protects MPNST cells in part by
162 neutralizing soluble AOs to safeguard HSP60 and the mitochondrial proteome (Figure 2I).
163
164 **MPNST cells react to HSF1 deficiency by activating JNK to attenuate translation**
165 Given their dependency on HSF1, cancer cells are expected to mount certain responses to
166 survive and adapt to the lethal HSF1 inhibition. Previously, we uncovered that in *Hsf1*-deficient
167 mice, the stress-responsive JNK kinase becomes constitutively activated, which, in turn,
168 disassembles mTORC1.[33] JNK does so by phosphorylating both RAPTOR and mTOR, two core
169 components of mTORC1. This mTORC1 inhibition diminishes protein translation, leading to
170 reduced cell size and whole-body lean mass in *Hsf1*-deficient mice.[33]
171
172 We reasoned that cancer cells might exploit this molecular regulation for their survival and
173 adaptation. In MPNST cells *HSF1* knockdown activated JNK, indicated by elevated JNK
174 T183/Y185 phosphorylation; in parallel to JNK activation, there was mTORC1 inhibition,
175 evidenced by diminished p70S6K T389 phosphorylation and 4EBP1 S65/T70 phosphorylation
176 (Figures 3A, 3B, and S3A-S3D).[34,35] In contrast, *HSF*1 knockdown minimally affected JNK and
177 mTORC1 in HSCs (Figures 3A and 3B). Detected by PLA, in MPNST cells HSF1 interacted
178 with JNK; however, *HSF1* depletion promoted JNK-RAPTOR interactions but diminished
179 mTOR-RAPTOR interactions simultaneously (Figures 3C-3E). The mTOR-RAPTOR interaction
180 is essential to the assembly and activity of mTORC1.[36] Thus, these findings support that JNK
181 senses HSF1 deficiency to repress mTORC1. Of interest, compared to non-transformed cells,
182 this sensing mechanism appears more prominent in malignant cells.
183

184 As expected for mTORC1 inhibition, *HSF1* depletion reduced global protein translation rate in
185 MPNST cells (Figures 3F, S3E, and S3F), detected by puromycin labeling as described
186 previously.[33,37] Beyond MPNST cells, this regulation of translation by HSF1 was conserved in
187 diverse human cancer cell lines (Figure 3G). Importantly, treatment with JNK-IN-8, an
188 irreversible JNK inhibitor,[38] largely rescued this impaired protein translation owing to *HSF1*
189 depletion (Figures 3F, S3E, and S3F). Interestingly, JNK inhibition augmented the basal
190 translation rate as well. Consistent with these findings, in human cancers higher *HSF1*
191 expression is associated with lower JNK activation (Figure S3G); in turn, lower JNK activation
192 is accompanied by higher mTORC1 activity, reflected by higher 4EBP1 Ser65 phosphorylation
193 (Figure S3H). In aggregate, our findings demonstrate that JNK activation is causally linked to
194 inhibition of mTORC1 and translation. Therefore, through JNK suppression HSF1 permits
195 robust protein translation, which is fundamental to malignant growth (Figure 3H).
196
197 **Lessening protein quantity is an adaptive response to alleviate proteomic instability**
198 We next asked why cells respond to HSF1 deficiency by attenuating translation. While HSF1
199 controls protein quality via HSPs, mTORC1 governs protein quantity via translation. It would be
200 beneficial to lower protein quantity when protein quality is jeopardized. Thus, we reasoned that
201 this regulation might represent a cellular adaptive response to imbalanced protein quantity and
202 quality engendered by HSF1 deficiency.
203
204 Proteomic imbalance disrupts proteome homeostasis and contributes to proteomic instability,
205 which may ultimately trigger amyloidogenesis. To inflict proteomic imbalance, we first
206 stimulated protein translation in MPNST cells by inhibiting JNK. As expected, JNK-IN-8

207 reduced the phosphorylation of c-JUN, a canonical substrate of JNK,[34] in MPNST cells (Figure
208 4A). In support of enhanced protein translation, JNK-IN-8 further activated mTORC1 in these
209 cells (Figures 4A and S4A); in contrast, marginal effects were observed in HSCs (Figure 4B).
210 Congruently, JNK-IN-8 did not significantly reduce c-JUN phosphorylation in HSCs, supporting
211 a lack of JNK activation in these non-transformed Schwann cells. Intriguingly, the heightened
212 protein translation following JNK inhibition was accompanied by elevated amyloid levels in
213 MPNST cells (Figures 4C and S4B). On the contrary, there were no significant changes in
214 amyloid levels in HSCs (Figure 4D).
215
216 To determine the role of protein translation in amyloidogenesis, we chose to block translation
217 using two pharmacological inhibitors, 4EGI-1 and LY2584702, with distinct mechanisms of
218 action. While 4EGI-1 disrupts eIF4E-eIF4G interactions,[39] LY2584702 inhibits p70S6K.[40]
219 Interestingly, both inhibitors diminished the basal amyloid levels in MPNST cells (Figures
220 4E,4F, and S4C), revealing a causal relationship between protein translation and
221 amyloidogenesis. Importantly, translation inhibition also blocked the induction of amyloids by
222 JNK-IN-8 in MPNST cells (Figures 4G, 4H, S4D, and S4E), indicating that JNK suppresses
223 amyloidogenesis via translation inhibition. No significant effects were observed in HSCs
224 (Figures 4G and 4H).
225
226 Considering the role of translation in amyloidogenesis, we reasoned that preventing translation
227 attenuation would aggravate proteomic imbalance and enhance cytotoxicity in malignant cells.
228 As expected, JNK-IN-8 further elevated the amyloid levels in MPNST cells following *HSF1*
229 depletion, which was accompanied by exacerbated apoptosis, detected by caspase 3 cleavage

230 (Figures 4I, 4J, and S4F).[41] Importantly, CR treatment blocked apoptosis, detected by PARP
231 cleavage (Figure S4G),[42] causally implicating amyloidogenesis. In contrast, *HSF1* depletion and
232 JNK inhibition exerted no significant impacts on non-transformed Schwann cells (Figures 4K
233 and 4L). Thus, our findings support that proteomic imbalance in malignant cells contributes to
234 proteomic instability and amyloidogenesis. In stark contrast, there is no or little amyloidogenesis
235 in non-transformed cells, owing to their balanced protein quantity and quality. Moreover,
236 through translation attenuation, malignant cells attempt to survive and adapt to proteomic
237 imbalance (Figure 4M).
238
239 **mTORC1 stimulation aggravates proteomic imbalance and cytotoxicity induced by HSF1**
240 **inhibition**
241 Apart from mTORC1, JNK regulates many other targets. To stimulate mTORC1 and protein
242 translation specifically, we next genetically inhibited the tumor suppressor Tuberous Sclerosis
243 Complex subunit 2 (*TSC2*), a key negative regulator of mTORC1,[43] in MPNST cells. As
244 expected, knocking down *TSC2* in MPNST cells promoted phosphorylation of both p70S6K and
245 4EBP1, which was accompanied by elevated amyloids (Figures S5A-S5F). Like genetic *HSF1*
246 depletion, pharmacological inhibition of HSF1 by DTHIB elevated global protein
247 polyubiquitination and amyloids in MPNST cells (Figures 5A, 5B, and S5G), eliciting proteomic
248 instability. The newly developed small-molecule inhibitor DTHIB directly binds to the DNA-
249 binding domain of HSF1 and potently blocks the HSF1-mediated transcription.[44] Compared to
250 control cells, HSF1 inhibition by DTHIB induced considerably higher levels of amyloids in
251 *TSC2*-deficient MPNST cells (Figure 5B). Of note, *TSC2*-deficient cells displayed more
252 profound JNK activation and mTORC1 inhibition following DTHIB treatment, reflecting a

253 cellular response to severe proteotoxic stress. Consistently, compared to slight or intermediate
254 cytotoxicity in control MPNST cells, detected by plasma membrane permeabilization, *TSC2*-
255 deficient cells were highly sensitive to HSF1 inhibition (Figures 5C, 5D, and S5H-S5K).
256 Importantly, either translation inhibition or CR treatment largely blocked this cytotoxicity
257 (Figures 5C and 5D), causally implicating amyloidogenesis. In support of a role of HSF1 in
258 enabling *TSC2* deficiency, among patients whose tumors harbor *TSC2* deletion higher *HSF1*
259 gene expression is correlated with shortened survival (Figure S5L).
260
261 To exclude possible mTORC1-independent effects of *TSC2* deficiency, we alternatively fed cells
262 with NV-5138, a leucine analog currently under clinical trials as an antidepressant.[45,46]Amino
263 acids, particularly leucine, are potent activators of mTORC1.[47] Of interest, whereas NV-5138 is
264 capable of activating mTORC1, it cannot be utilized for protein synthesis.[45,46] To maximize
265 mTORC1 stimulation *ex vivo*, cells were cultured in leucine-free medium. Like *TSC2*
266 knockdown, NV-5138 stimulated mTORC1 and heightened amyloid levels in MPNST cells
267 (Figures 5E and 5F); however, it only elicited pronounced cytotoxicity with concurrent HSF1
268 inhibition (Figure 5G). Again, CR treatment largely blocked this cytotoxicity (Figure 5G). In
269 sharp contrast, combined NV-5138 and DTHIB treatment did not significantly impact non-
270 transformed Schwann cells (Figure 5H). Of interest, their mTORC1 signaling was less
271 responsive to NV-5138 stimulation (Figures 5I). Collectively, these findings indicate that
272 mTORC1 stimulation synergizes with HSF1 inhibition to rapidly trigger severe cytotoxicity in
273 MPNST cells, in part by prompting unconstrained proteomic imbalance and amyloidogenesis.
274
275 **Unconstrained proteomic imbalance incites non-apoptotic, non-autophagic death**

276 HSF1 inhibition alone induced both apoptotic and non-apoptotic death in MPNST cells,
277 distinguished by caspase 3 cleavage; intriguingly, concurrent mTORC1 stimulation caused a
278 striking shift towards non-apoptotic cell death, characterized by cell membrane permeabilization
279 without caspase 3 cleavage (Figures 6A and 6B).
280
281 To date, several forms of non-apoptotic cell death have been described, including pyroptosis,
282 necroptosis, ferroptosis, and autophagic death, all of which could result in loss of cell membrane
283 integrity. Corroborating a non-apoptotic mechanism, the pan-caspase inhibitor Q-VD-OPh did
284 not prevent the membrane permeabilization in *TSC2*-deficient MPNST cells treated with DTHIB
285 (Figures 6A and 6B).[48] However, it did block the apoptosis in control MPNST cells treated with
286 DTHIB (Figures 6A and S6A). As Q-VD-OPh inhibits caspase 1 and no caspase 1 cleavage was
287 detected (Figure S6B),[49] a key driver of pyroptosis,[50] this result does not support a pyroptotic cell
288 death either. Similarly, HSF1 inhibition did not induce necroptosis in *TSC2*-deficient MPNST
289 cells, evidenced by the lack of MLKL Ser358 phosphorylation (Figure S6B), an essential event
290 executing necroptosis.[51] Congruently, the necroptosis inhibitor necrostatin-1 exerted no effects
291 on the cell membrane disruption (Figures 6C and S6C).[51]
292
293 Intriguingly, HSF1 inhibition diminished glutathione peroxidase 4 (GPX4) but increased
294 transferrin receptor 1 (TFR1), which was accompanied with markedly elevated lipid
295 peroxidation, in *TSC2*-deficient MPNST cells (Figures 6D and S6D). All these changes are
296 indicative of ferroptosis.[52,53] Although in *TSC2*-deificent cells liproxstatin-1, a potent ferroptosis
297 inhibitor,[52,53] reversed the elevation of TFR1 elicited by the ferroptosis inducer erastin, it neither
298 blocked the marked increase in TFR1 nor stopped the membrane disruption induced by DTHIB

299 (Figures 6C, 6D, and S6C). Similarly, HSF1 inhibition also elicited autophagy, evidenced by
300 diminished p62/SQSTM1 and elevated LC3B-II (Figure 6E).[54] To determine whether autophagic
301 cell death was implicated, we employed the class III PI3K inhibitor wortmannin to block
302 autophagy.[55] As expected, wortmannin effectively prevented the decreases in p62/SQSTM1 and
303 LC3B-II induced by rapamycin in *TSC2*-deficient MPNST cells (Figure 6E), indicating
304 successful blockade of autophagy. Nevertheless, wortmannin failed to block the cell membrane
305 disruption in *TSC2*-deficient cells treated with HSF1 inhibitors (Figures 6F and S6E). These
306 findings suggest that both ferroptosis and autophagy are the consequences, rather than the
307 causes, of cell membrane disruption. Collectively, our findings support that uncontained
308 amyloids potently trigger cell death, which is neither apoptotic nor autophagic (Figure 6G).
309
310
311
312
313
314
315
316
317
318
319
320
321

322 **DISCUSSIONS**

323 Genomic instability has been broadly recognized as a driver of oncogenesis. In contrast, the
324 implications of proteomic instability in cancer remain obscure.

325

326 **Proteomic instability is tumor suppressive but inevitable**

327 Proteomic instability does occur in cancer, evidenced by elevated protein polyubiquitination,
328 aggregation, and even amyloidogenesis. In cancer, proteomic instability can be ascribed to
329 several mechanisms, including protein oxidation by reactive oxygen species, protein misfolding
330 owing to genetic mutations, and augmentation of protein dosage caused by aneuploidy.[1,3]
331 Revealed by our recent studies, uncontrolled protein translation also contributes to
332 amyloidogenesis. This is not entirely surprising, as it has been estimated that up to 30% of all
333 newly synthesized polypeptides are misfolded and subjected to proteasomal degradation.[56]
334 Imaginably, aberrant protein synthesis would increase the chance of producing protein
335 aggregates and even amyloids, especially considering numerous genetic mutations affecting
336 protein folding in cancer cells. Ironically, dysregulated protein translation is fundamental to
337 malignant growth, making proteomic instability and amyloidogenesis inevitable.

338

339 At the cellular level, amyloids are toxic to both neurons and cancer cells. At the organismal
340 level, amyloidogenesis is neurodegenerative but tumor suppressive. Mechanistically, our studies
341 demonstrate that soluble AOs can directly attack the guardian of the mitochondrial proteome
342 HSP60. Of course, mechanisms other than targeting HSP60 exist as well. Moreover, it remains to
343 be elucidated what other proteins comprise cancer-associated amyloids, in addition to the
344 Alzheimer's disease-associated Aβ.

345

346 **HSF1 contains proteomic instability to enable malignancy**

347 The multifaceted pro-oncogenic roles of HSF1 have been ascribed to a wide array of underlying
348 mechanisms; nonetheless, a universal one remains to be defined.

349

350 As an inevitable price of malignancy, proteomic instability must be contained by cancer cells to
351 avert tumor suppression and sustain malignant phenotypes. Now, our findings reveal that HSF1
352 contains proteomic instability, particularly amyloidogenesis, constituting a generic pro-
353 oncogenic mechanism. It is worth noting that HSF1 only contains and mitigates, but cannot
354 eradicate, amyloidogenesis, as uncontrolled protein translation is a direct cause of
355 amyloidogenesis in cancer cells. This dependency on HSF1 to contain proteomic instability
356 partly underlies the phenomenon of "HSF1 addiction of cancer".

357

358 Our studies further support that HSF1 contains amyloidogenesis via at least two mechanisms,
359 direct and indirect. On the one hand, through induction of HSPs, HSF1 ensures appropriate
360 protein folding to maintain a healthy proteome, thereby preventing the emergence of amyloids.
361 This is supported by the finding that HSF1 inhibition heightens protein ubiquitination,
362 aggregation, and amyloidogenesis. On the other hand, HSF1 can neutralize soluble AOs directly
363 once they emerge. Under this context, HSF1 inhibition would unleash AOs to assault HSP60,
364 inflicting mitochondrial damage and toxicity. Thus, in cancer cells HSF1 inhibition both enlarges
365 the quantity of amyloids and, more importantly, renders them toxic.

366

367 **mTORC1 signaling becomes tumor suppressive in the absence of HSF1**

368 Given the dependency of malignant growth on protein translation, unsurprisingly, mTORC1
369 signaling is hyperactive in human cancers, which is, canonically, considered oncogenic.[57,58]
370 Consistently, 4EBP1 Ser65 phosphorylation, indicative of mTORC1 activation, in tumor tissues
371 is correlated with shortened patients' survival (Figure S6F).
372
373 Unexpectedly, our current studies reveal that mTORC1 signaling becomes tumor suppressive in
374 the absence of HSF1, owing to profound disproportion between protein quantity and quality.
375 This unconstrained proteomic imbalance, in turn, exacerbates proteomic instability and tumor-
376 suppressive amyloidogenesis. The notable blockage of cytotoxicity by either translation
377 inhibitors or CR lends strong support to this model. Conceptually, HSF1 empowers the
378 oncogenic potential of mTORC1 signaling, reinforcing HSF1 as an oncogenic enabler. In line
379 with this notion, co-upregulation of *HSF1* mRNA and mTORC1 activity is significantly
380 associated with shortened patients' survival (Figure S6G).
381
382 **Driving proteomic imbalance represents a new therapeutic concept**
383 Currently popular chemo-and radiotherapies mainly target the cancer genome, causing DNA
384 damage. A new horizon in cancer therapy is targeting the cancer proteome. To date, much effort
385 has been devoted to inhibiting individual HSP families, such as HSP70 and HSP90.[59,60]
386 However, every cell is equipped with both constitutive and inducible HSPs. While the former
387 comprise the basal chaperoning capacity that is essential to life, the latter supply the extra
388 chaperoning capacity, which is dispensable for normal life and only required under stressful
389 conditions. Their structural and functional resemblances pose the biggest challenge for small
390 molecules to distinguish these cognate HSPs. Moreover, multiple families of HSPs, including

391 HSP100, HSP90, HSP70, HSP60, HSP40, and small HSPs, exist inside cells. Targeting single
392 HSP family would have limited therapeutic effects. Thus, new approaches or directions are
393 warranted to overcome these drawbacks.
394
395 Our and others' studies collectively support that malignant cells constantly endure intrinsic
396 proteotoxic stress, rendering HSF1 constitutively active. In turn, cancer cells become reliant on
397 the extra chaperoning capacity, conferred by HSF1, for their growth and survival. Thus, only
398 eliminating this extra chaperoning capacity but sparing the basal one would be an ideal strategy
399 to combat malignancy. Together, these concepts provide strong rationales for targeting HSF1 in
400 cancer. It is exciting to witness the recent launch of HSF1 inhibitors into clinical trials.[61]
401
402 In reaction to HSF1 inhibition, unsurprisingly, cancer cells attenuate protein synthesis. This
403 adaptive response underscores the importance of balanced protein quantity and quality to cellular
404 fitness, a key concept inspiring us to explore driving proteomic imbalance for cancer therapy. Of
405 note, breaking this adaptation may impede tumor evolution.
406
407 The widespread hyperactivation of mTORC1 in human cancers makes it an attractive therapeutic
408 target. Hence, an array of mTOR inhibitors have been developed, several of which are actively
409 under clinical evaluation.[58,62] Thus far, these inhibitors have displayed mostly cytostatic effects
410 and less than expected therapeutic efficacies.[62,63] Considering the essentiality of protein
411 translation to life, profound mTORC1 inhibition would inflict undesirable toxicities in normal
412 cells and tissues. In fact, mTORC1 inhibitors have long been known as immunosuppressants.[62,64]
413

414 Counterintuitively, we stimulated mTORC1 to drive proteomic imbalance, opposite to the
415 prevailing strategy in cancer therapy. mTORC1 stimulation, when combined with HSF1
416 inhibition, engendered prominent cytotoxic effects (Figure 6H), representing a key therapeutic
417 benefit. Moreover, this amyloid-dependent cell death offers a large therapeutic window, owing to
418 the lack of amyloidogenesis in primary cells. Thus, using the *NF1*-deficient MPNST model
419 system, we herein accomplished the proof-of-concept experiment to demonstrate the feasibility
420 of driving proteomic imbalance in cancer. Noteworthily, this therapeutic concept should be
421 applicable to a broad spectrum of human cancers, beyond this specific NF1-associated
422 malignancy.
423
424
425
426
427
428
429
430
431
432
433
434
435
436

ACKNOWLEDGMENTS

We would like to thank the Optical Microscopy and Image Analysis lab (OMAL) for their assistance with the confocal microscopy studies. Schematic illustrations are created with BioRender.com. This work was supported by the grant from Department of Defense Congressionally Directed Medical Research Programs to C.D. (NF150028) and by the Intramural Research Program of the NIH, National Cancer Institute, Center for Cancer Research (1ZIABC011767). The content of this publication does not necessarily reflect the views or policies of the Department of Health and Human Services, nor does mention of trade names, commercial products, or organizations imply endorsement by the U.S. government.

AUTHOR CONTRIBUTIONS: B.M.R. and K-H.C. designed and conducted the experiments. C.D. conceptualized and supervised this study and analyzed the results. B.M.R. and C.D. wrote the manuscript.

DECLARATION OF INTERESTS: The authors declare no competing interests.

460 **EXPERIMENTAL MATERIALS AND METHODS**

461 **Cells, Chemicals, and reagents**

462 S462 (female) and 90-8TL (female) cells were kindly provided by Dr. Karen Cichowski.
463 sNF96.2 cells (male) and immortalized human Schwann cells (hTERT ipn02.3 2λ, female) were
464 purchased from ATCC. Primary human Schwann cells (Cat#1700, ScienCell Research
465 Laboratories) were grown on poly-L-lysine coated T-75 flasks and maintained in complete
466 Schwann Cell Medium (Cat#1701, ScienCell Research Laboratories). All cell lines, except 90-
467 8TL and HSCs (no known STR profiles available), were authenticated by ATCC. All cell lines,
468 except primary human Schwann cells, were maintained in DMEM supplemented with 10%
469 HyClone bovine growth serum and 1% penicillin–streptomycin. Cells were maintained in an
470 incubator with 5% CO2 at 37 °C.

471

472 The following chemicals were purchased from commercial sources: JNK-IN-8 (Cat#S4901,
473 Selleckchem), 6-FAM-dC-puromycin (cat#NU-925-6FM, Jena Bioscience), Congo red
474 (cat#B2431014, Thermo Scientific Chemicals), Thioflavin T (cat#211760050, Thermo Scientific
475 Chemicals), LY2584702 (cat#S7698, Selleckchem), 4EGI-1 (cat#S7369, Selleckchem), and
476 DTHIB (cat# HY-138280, MedChemExpress), Q-VD-OPh (cat#HY-12305, MedChemExpress),
477 necrostatin-1 (cat#HY-15760, MedChemExpress), Liproxstatin-1 (cat#HY-12726,
478 MedChemExpress), wortmannin (cat#HY-10197, MedChemExpress), rapamycin (cat#HY-
479 10219, MedChemExpress), erastin (cat#HY-15763, MedChemExpress), MHY1485 (cat#HY-
480 B0795, MedChemExpress), NV-5138 HCl (cat#HY-114384B, MedChemExpress), and Liperfluo
481 (cat#L248, Dojindo Laboratories).

482

483 Rabbit phospho-4EBP1 S65/T70 antibody (cat#sc-12884-R), mouse monoclonal HSF1 (E-4,
484 cat#sc-17757) antibody, rabbit HSF1 antibody (H-311, cat#sc-9144), mouse monoclonal JNK
485 (D-2, cat#sc-7345), rabbit JNK1/3 (C-17, cat#sc-474) antibody were purchased from Santa
486 Cruz Biotechnology; antibodies for phosphor-4EBP1 Thr70 (cat#9455), phospho-4EBP1
487 Thr37/46 (236B4, cat#2855), phospho-p70S6K T389 (108D2, cat# 9234), phosphor-S6RP
488 Ser235/236 (D57.2.2E, cat#4858), p70 S6K (49D7, cat#2708), 4EBP1 (53H11, cat#9644),
489 S6RP (5G10, cat#2217), mTOR (7C10, cat#2983), phospho-JNK1/2 T183/Y185 (81E11,
490 cat#4668), JNK2 (56G8, cat#9258), c-Jun (60A8, cat#9165), phospho-c-Jun Ser63 II
491 (cat#9261), PARP (cat#9542), Tuberin/TSC2 (D93F12, cat#4308), SQSTM1/p62 (D1Q5S,
492 cat#39749), cleaved caspase 3 (Asp175) (5A1E, cat#9664), caspase 1(D7F10, cat#3866),
493 gasdermin D (E9S1X, cat#39754), phosphor-MLKL Ser358 (D6H3V, cat#91689), GPX4
494 (E5Y8K, cat#59735), and transferrin receptor/CD71 (H68.4, cat#46222) antibody were
495 purchased from Cell Signaling Technologies; mouse β-actin antibody-HRP (Cat#A00730)
496 conjugates were from GenScript. Anti-K48-specific ubiquitin antibody (Apu2, cat#05-1307)
497 and mouse monoclonal anti-RAPTOR antibody (1H6.2, cat#05-1470) were purchased from
498 EMD Millipore. Mouse monoclonal anti-JNK1 (C-terminal region) antibody (cat#JM2671)
499 was purchased from ECM Biosciences. Anti-amyloid oligomers (A11, cat#SPC-506D) and
500 anti-amyloid fibrils (OC, cat#SPC-507D) antibodies were purchased from StressMarq
501 Biosciences Inc. Mouse monoclonal anti-HSP60 antibody (LK-1, cat#ADI-SPA-806) was
502 purchased from Enzo Life Sciences Inc. β-Actin (cat#GTX629630), GAPDH
503 (cat#GTX627408), α-tubulin (GT114, cat#GTX628802), and LC3B antibody
504 (cat#GTX127375) was purchased from GeneTex Inc.
505

506 **METHOD DETAILS**

507 **Lentiviral Particle Production and Transduction of lentiviral shRNAs**

508 Lentiviral pLKO.1 shRNA plasmids targeting human *HSF1* were described previously[10]:
509 TRCN0000007480 (hA6) and TRCN0000007483 (hA9). The sequence of control hairpins
510 targeting a scrambled sequence with no known homology to any human genes is 5′-
511 CCTAAGGTTAAGTCGCCCTCG-3′. The pLKO.1 shRNA plasmid targeting human *TSC2* was
512 a gift from Do-Hyung Kim (Cat#15478, Addgene). Lentiviral pLKO shRNA plasmids were
513 transiently co-transfected individually along with plasmids encoding ΔVPR and VSV-G into
514 HEK293T cells using TurboFect™ (Cat#R0531, Thermo Scientific). Viral supernatants were
515 collected after centrifugation at 1,000 rpm for 15 min. Viral transduction was achieved by
516 incubating target cells with viral supernatants containing 10μg/ml polybrene (Cat#TR-1003-G,
517 Millipore-Sigma) for 24h. For stable knockdown of *TSC2,* lentivirus particles were prepared using
518 pLKO shRNA plasmids targeting human *TSC2*. Scrambled shRNA was used for stable control
519 cells. After 4 days of transduction, cells were gradually selected using 1-4 μg/ml puromycin for 2
520 weeks.

521 **Soluble and Insoluble Protein Fractionation**

522 Equal numbers of cells were incubated with cold cell-lysis buffer (100 mM NaCl, 30 mM Tris-
523 HCl pH 7.6, 1% Triton X-100, 20 mM sodium fluoride, 1mM EDTA, 1mM sodium
524 orthovanadate, and 1x Halt™ protease inhibitor cocktail) on ice for 20 min. The crude lysates
525 were first centrifuged at 500xg for 5 min at 4°C. The supernatants from low-speed (500xg)
526 centrifugation were transferred to a new Eppendorf tube. The first pellets were resuspended in

527 DNA digestion solution (2 units DNase I, 1% Triton X-100, 10 mM Tris-HCl, 2.5 mM
528 MgCl2, 0.5 mM CaCl2, pH 7.6) for 30 min at RT. An equal volume of 1xPBS with 2% SDS
529 was then added to resuspend the first pellets for additional 30 min at RT. Following the
530 centrifugation at 17,000xg for 10 min at RT, the supernatants were removed. The supernatants
531 from low-speed centrifuge were added back to the second pellets, followed by centrifugation
532 at 17,000xg for 15 min at 4°C. The final supernatants and pellets from high-speed (17,000xg)
533 centrifugation were collected as detergent-soluble and -insoluble fractions, respectively.
534 Insoluble fractions were further sonicated in 1xPBS with 2% SDS at high intensity using a
535 Bioruptor® Sonication Device (Diagenode) for SDS-PAGE.

536 **ThT and CR Staining for Flow Cytometry**

537 After washing with 1xPBS, cells were fixed with 4% formaldehyde at RT for 10 min.
538 Following fixation and 1xPBS washing, cells were resuspended in 1 ml permeabilization
539 buffer (1xPBS with 0.5% Triton X-100 and 3 mM EDTA) and incubated on ice for 30 min.
540 Following washing with 1xPBS, Cells were stained with 10 μM ThT or CR dissolved in
541 1xPBS for 5 min. Cells were washed and resuspended in PBS and fluorescence signals were
542 measured by a FACSCalibur, LSRFortessa X-20 or LSR II flow cytometer (BD Biosciences).

543 **Amyloid Oligomer and Fibril Quantitation by Direct ELISA and Flow Cytometry**

544 To quantitate soluble amyloid prefibrillar oligomers, soluble cell lysates diluted in 1xPBS
545 from equal numbers of cells were coated on each well in a 96-well ELISA plate at 4°C
546 overnight followed by blocking (5% non-fat milk in TBS-0.05% Tween® 20) at RT for 1 hr.
547 Each well was incubated with 100 μl amyloid oligomer antibodies (A11, 1:1,000 diluted in

548 the blocking buffer) at RT for 2 hr. After washing with TBS-T, goat anti-rabbit secondary Ab
549 HRP conjugates (1:1,000 diluted in blocking buffer) were added to each well and incubated at
550 RT for 1 hr. Following washing, 100 µl 1-Step Ultra TMB-ELISA substrates (Cat#34029,
551 Thermo Scientific) were added to each well. After adding 100µl Stop solution, absorbance was
552 measured at 450 nm using a SpectraMax iD5 microplate reader (Molecular Devices).

553 To quantitate amyloid fibrils, detergent-insoluble fractions from equal numbers of cells were
554 extracted as described in Soluble and Insoluble Protein Fractionation. The final pellets were
555 collected as detergent-insoluble fractions and solubilized by sonication for 15 min in 1xPBS
556 with 2% SDS. Solubilized proteins diluted in 1xPBS were added to each well and incubated at
557 37°C without cover overnight to air dry the wells. The following steps were identical to the
558 oligomer detection except for the use of amyloid fibril antibodies (OC) as the primary Ab.

559 For amyloid oligomer and fibril quantification by flow cytometry, cells were collected by
560 trypsinization and fixed in 4% Formaldehyde at RT for 10 min. Following permeabilization using
561 0.3% Triton-X-100, samples were incubated with primary antibodies A11-FITC (1:100 in 5%
562 BSA, StressMarq Biosciences, cat# SPC-506D-FITC) or OC-PerCP (1:100 in 5% BSA,
563 StressMarq Biosciences, cat# SPC-507D-PCP) at RT for 3 hrs. The cells were washed with PBS
564 and analyzed using flow cytometry.

565

566 **Measurement of Cell Viability**

567 Cell viability was determined using the CellTiter-Blue® Cell Viability Assay (cat#G8080,
568 Promega). Cells were grown in 96 well plates (1×10^4 per well) for 24h. A 20µl CellTiter-Blue®
569 reagent was added to 100µl of media in each well. The plates were incubated for 2h at 37°C and

570 the fluorescence was recorded at 560/590 nm. The reagents were discarded, and the wells were
571 washed with PBS before adding fresh media. Similarly, subsequent readings were recorded at
572 24h intervals till 96h time point.
573
574 **Proximity Ligation Assay**
575 Cells were fixed with 4% formaldehyde in PBS for 15 min at RT. After blocking with 5% normal
576 goat serum in PBS with 0.3% Triton X-100, primary antibodies 1:100 diluted in blocking buffer
577 were incubated with fixed cells overnight at 4°C. Following washing with PLA wash Buffer A,
578 samples were incubated with 1:5 diluted Duolink® in Situ PLA Probe anti-rabbit Plus
579 (cat#DUO92002, Sigma-Aldrich) and anti-mouse Minus (cat#DUO92004, Sigma-Aldrich) at
580 37°C for 1 hr. Subsequently, ligation (30 minutes, 37°C), rolling circle amplification, and detection
581 (120 minutes, 37°C) were performed using the Duolink® In Situ Detection Reagents Red
582 (cat#DUO92008, Sigma-Aldrich). Nuclei were counterstained with Hoechst 33342. PLA
583 signals were documented by a Zeiss LSM780 confocal microscope (Carl Zeiss). For PLA flow
584 cytometry, an equal number of cells were collected in microcentrifuge tubes by trypsinization and
585 fixed with 4% formaldehyde in PBS for 10 min at RT. Subsequent PLA steps were followed as
586 described earlier. The PLA signals were quantified by a FACSCalibur flow cytometer (BD
587 Biosciences).
588
589 Mouse anti-JNK1 (JM2671) and rabbit anti-HSF1 (H-311) antibodies were used for JNK-HSF1
590 PLA. Rabbit anti-JNK1/3 (C-17) and mouse anti-RAPTOR (1H6.2) antibodies were used for
591 JNK-RAPTOR PLA. Rabbit anti-mTOR (7C10) and mouse anti-RAPTOR (1H6.2) antibodies
592 were used for mTOR-RAPTOR PLA. Mouse anti-HSF1 (E-4) and rabbit anti-AO (A11)

593 antibodies were used for HSF1-AO PLA. Rabbit anti-AO (A11) and mouse anti-HSP60 (LK1)
594 antibodies were used for AO-HSP60 PLA.

595 **Measurement of global protein translation**

596 Live cells were incubated with 100 nM 6-FAM-dC-puromycin in complete culture medium
597 for 30 min and analyzed by a FACSCalibur flow cytometer (BD Biosciences).

598 **Immunoblotting and Immunoprecipitation**

599 Whole-cell protein extracts were prepared in cold cell-lysis buffer (100 mM NaCl, 30 mM Tris-
600 HCl pH 7.6, 1% Triton X-100, 20 mM sodium fluoride, 1mM EDTA, 1mM sodium
601 orthovanadate, and 1x Halt™ protease inhibitor cocktail). Proteins were transferred to
602 nitrocellulose membranes. Following incubation with the blocking buffer (5% non-fat milk in 1x
603 TBS-T) for 1 hour at RT, membranes were incubated with primary antibodies (1:1,000 dilution in
604 the blocking buffer) overnight at 4 °C. After washing with 1xTBS-T for 3 times, membranes
605 were incubated with peroxidase-conjugated secondary antibodies (1: 3,000 diluted in the
606 blocking buffer) at RT for 1 hr. Signals were detected using SuperSignal™ West
607 chemiluminescent substrates. For normal Co-IP, proteins were extracted using a QSonica Q125
608 sonicator (total process time: 15S, pulse-on time: 5S, pulse-off time: 10S, output intensity: 30%)
609 in 1x sonication buffer (20 mM Tris, 20 mM NaCl, 1 mM EDTA, 20 mM β-glycerol-phosphate,
610 20 mM sodium fluoride, 4 mM sodium orthovanadate, and 1 mM DTT pH7.4, supplemented
611 with Halt protease inhibitor cocktail). Total 1 mg whole cell lysates were incubated with A11
612 antibodies at 4 °C overnight. Normal rabbit IgG were used as the negative controls. The primary
613 antibody was precipitated using Protein G magnetic beads. After washing with the lysis buffer
614 for 3 times, beads were boiled in 1x loading buffer for 5 min before loading on SDS-PAGE.

615 EasyBlocker (Cat#GTX425858, GeneTex) was used for blocking and anti-HSF1 (H-311)
616 primary antibody (cat#sc-9144, Santa Cruz Biotechnology) incubation (1:1,000, O/N at 4°C).
617 The blot was incubated with EasyBlot anti-Rabbit IgG HRP conjugated antibody
618 (cat#GTX221666-01, GeneTex) for 1 hour. Chemiluminescent signals were captured by an
619 iBright™ FL1000 imaging system (ThermoFisher Scientific).
620

621 **Live-Or-Dye™ Dead Cell Staining**

622 Cells were cultured in DMEM for 48 hours before being treated with inhibitors for the required
623 periods and collected by trypsinization. $1x10^6$ cells/ml cells were stained with Live-or-Dye™
624 fixable dead cell dyes (1:1,000 dilution, cat#32016, Biotium) at RT for 30 min, protected from
625 light. Stained cells were washed once with PBS and analyzed by flow cytometry. For co-staining
626 with cleaved caspase 3 antibody, stained cells were fixed with 4% formaldehyde (10 min, RT)
627 and permeabilized with 0.3% Triton-X-100 in PBS (10 min, RT). The cells were stained by
628 Cleaved Caspase 3 antibody (Asp175) (5A1E) (1:1,000, cat#9664, Cell Signaling Technology)
629 followed by goat anti-Rabbit IgG Alexa Fluor™ 488 conjugated (1:1,000, cat#A-11034,
630 ThermoFisher Scientific) secondary antibodies. The samples were analyzed by flow cytometry.

631 **Inhibitor treatments**

632 Treatments with DTHIB, Q-VD-OPh, Liproxstatin-1, Necrostatin-1, and Wortmannin were
633 done for 72 hours. For Congo Red and LY-2584702 treatments, cells were pretreated for 24h
634 followed by DTHIB for an additional 72h. For treatments with NV-5138, cells were pretreated
635 for 48 hours in a leucine-free DMEM (cat#226-024, Crystalgen) before adding DTHIB for an
636 additional 72 hours.
637

638

639 **Quantification And Statistical Analysis**

640 Statistical analyses were performed using Prism GraphPad 10.0 (GraphPad Software). The
641 detailed statistical methods and sample sizes are provided in the figure legends. All results are
642 expressed as mean±SD, mean±SEM, or median and IQR. The statistical significance is defined
643 as: *$p<0.05$, **$p<0.01$; ***$p<0.001$; ****$p<0.0001$; n.s.: not significant. For *in vitro*
644 experiments, sample size required was not determined a priori. The experiments were not
645 randomized**.**

646

647

648

649

650

651

652

653

654

655

656

657

658

659

660

661 **REFERENCES**

662 1. Dai C, Dai S, Cao J. Proteotoxic stress of cancer: implication of the heat-shock response in
663 oncogenesis. J Cell Physiol. 2012;227(8):2982-7. doi: 10.1002/jcp.24017. PubMed PMID:
664 22105155; PMCID: PMC3431153.
665 2. Dai C. The heat-shock, or HSF1-mediated proteotoxic stress, response in cancer: from
666 proteomic stability to oncogenesis. Philos Trans R Soc Lond B Biol Sci. 2018;373(1738).
667 doi: 10.1098/rstb.2016.0525. PubMed PMID: 29203710; PMCID: PMC5717525.
668 3. Guang MHZ, Kavanagh EL, Dunne LP, Dowling P, Zhang L, Lindsay S, Bazou D, Goh CY,
669 Hanley C, Bianchi G, Anderson KC, O'Gorman P, McCann A. Targeting Proteotoxic Stress
670 in Cancer: A Review of the Role that Protein Quality Control Pathways Play in Oncogenesis.
671 Cancers (Basel). 2019;11(1). Epub 20190109. doi: 10.3390/cancers11010066. PubMed
672 PMID: 30634515; PMCID: PMC6356294.
673 4. Wilson DM, 3rd, Cookson MR, Van Den Bosch L, Zetterberg H, Holtzman DM, Dewachter
674 I. Hallmarks of neurodegenerative diseases. Cell. 2023;186(4):693-714. doi:
675 10.1016/j.cell.2022.12.032. PubMed PMID: 36803602.
676 5. Tang Z, Dai S, He Y, Doty RA, Shultz LD, Sampson SB, Dai C. MEK guards proteome
677 stability and inhibits tumor-suppressive amyloidogenesis via HSF1. Cell. 2015;160(4):729-
678 44. doi: 10.1016/j.cell.2015.01.028. PubMed PMID: 25679764; PMCID: PMC4564124.
679 6. Li J, Labbadia J, Morimoto RI. Rethinking HSF1 in Stress, Development, and Organismal
680 Health. Trends Cell Biol. 2017;27(12):895-905. Epub 20170907. doi:
681 10.1016/j.tcb.2017.08.002. PubMed PMID: 28890254; PMCID: PMC5696061.
682 7. Anckar J, Sistonen L. Regulation of HSF1 function in the heat stress response: implications
683 in aging and disease. Annu Rev Biochem. 2011;80:1089-115. doi: 10.1146/annurev-

684 biochem-060809-095203. PubMed PMID: 21417720.

685 8. Gomez-Pastor R, Burchfiel ET, Thiele DJ. Regulation of heat shock transcription factors and
686 their roles in physiology and disease. Nat Rev Mol Cell Biol. 2018;19(1):4-19. Epub
687 20170830. doi: 10.1038/nrm.2017.73. PubMed PMID: 28852220; PMCID: PMC5794010.

688 9. Min JN, Huang L, Zimonjic DB, Moskophidis D, Mivechi NF. Selective suppression of
689 lymphomas by functional loss of Hsf1 in a p53-deficient mouse model for spontaneous
690 tumors. Oncogene. 2007;26(35):5086-97. Epub 20070219. doi: 10.1038/sj.onc.1210317.
691 PubMed PMID: 17310987.

692 10. Dai C, Whitesell L, Rogers AB, Lindquist S. Heat shock factor 1 is a powerful multifaceted
693 modifier of carcinogenesis. Cell. 2007;130(6):1005-18. doi: 10.1016/j.cell.2007.07.020.
694 PubMed PMID: 17889646; PMCID: PMC2586609.

695 11. Meng L, Gabai VL, Sherman MY. Heat-shock transcription factor HSF1 has a critical role in
696 human epidermal growth factor receptor-2-induced cellular transformation and
697 tumorigenesis. Oncogene. 2010;29(37):5204-13. Epub 20100712. doi:
698 10.1038/onc.2010.277. PubMed PMID: 20622894; PMCID: PMC2940982.

699 12. Jin X, Moskophidis D, Mivechi NF. Heat shock transcription factor 1 is a key determinant of
700 HCC development by regulating hepatic steatosis and metabolic syndrome. Cell Metab.
701 2011;14(1):91-103. doi: 10.1016/j.cmet.2011.03.025. PubMed PMID: 21723507; PMCID:
702 PMC3214631.

703 13. Dai C, Santagata S, Tang Z, Shi J, Cao J, Kwon H, Bronson RT, Whitesell L, Lindquist S.
704 Loss of tumor suppressor NF1 activates HSF1 to promote carcinogenesis. J Clin Invest.
705 2012;122(10):3742-54. Epub 20120904. doi: 10.1172/JCI62727. PubMed PMID: 22945628;
706 PMCID: PMC3461912.

707 14. Kourtis N, Lazaris C, Hockemeyer K, Balandran JC, Jimenez AR, Mullenders J, Gong Y,
708 Trimarchi T, Bhatt K, Hu H, Shrestha L, Ambesi-Impiombato A, Kelliher M, Paietta E,
709 Chiosis G, Guzman ML, Ferrando AA, Tsirigos A, Aifantis I. Oncogenic hijacking of the
710 stress response machinery in T cell acute lymphoblastic leukemia. Nat Med.
711 2018;24(8):1157-66. Epub 20180723. doi: 10.1038/s41591-018-0105-8. PubMed PMID:
712 30038221; PMCID: PMC6082694.
713 15. Fujimoto M, Takii R, Matsumoto M, Okada M, Nakayama KI, Nakato R, Fujiki K, Shirahige
714 K, Nakai A. HSF1 phosphorylation establishes an active chromatin state via the TRRAP-
715 TIP60 complex and promotes tumorigenesis. Nat Commun. 2022;13(1):4355. Epub
716 20220729. doi: 10.1038/s41467-022-32034-4. PubMed PMID: 35906200; PMCID:
717 PMC9338313.
718 16. Heimberger T, Andrulis M, Riedel S, Stuhmer T, Schraud H, Beilhack A, Bumm T, Bogen
719 B, Einsele H, Bargou RC, Chatterjee M. The heat shock transcription factor 1 as a potential
720 new therapeutic target in multiple myeloma. Br J Haematol. 2013;160(4):465-76. Epub
721 20121218. doi: 10.1111/bjh.12164. PubMed PMID: 23252346.
722 17. Chuma M, Sakamoto N, Nakai A, Hige S, Nakanishi M, Natsuizaka M, Suda G, Sho T,
723 Hatanaka K, Matsuno Y, Yokoo H, Kamiyama T, Taketomi A, Fujii G, Tashiro K, Hikiba Y,
724 Fujimoto M, Asaka M, Maeda S. Heat shock factor 1 accelerates hepatocellular carcinoma
725 development by activating nuclear factor-kappaB/mitogen-activated protein kinase.
726 Carcinogenesis. 2014;35(2):272-81. Epub 20131015. doi: 10.1093/carcin/bgt343. PubMed
727 PMID: 24130164.
728 18. Fujimoto M, Takaki E, Takii R, Tan K, Prakasam R, Hayashida N, Iemura S, Natsume T,
729 Nakai A. RPA assists HSF1 access to nucleosomal DNA by recruiting histone chaperone

730 FACT. Mol Cell. 2012;48(2):182-94. Epub 20120830. doi: 10.1016/j.molcel.2012.07.026.
731 PubMed PMID: 22940245.
732 19. Solimini NL, Luo J, Elledge SJ. Non-oncogene addiction and the stress phenotype of cancer
733 cells. Cell. 2007;130(6):986-8. doi: 10.1016/j.cell.2007.09.007. PubMed PMID: 17889643.
734 20. Gutmann DH, Ferner RE, Listernick RH, Korf BR, Wolters PL, Johnson KJ.
735 Neurofibromatosis type 1. Nat Rev Dis Primers. 2017;3:17004. Epub 20170223. doi:
736 10.1038/nrdp.2017.4. PubMed PMID: 28230061.
737 21. Hirbe AC, Gutmann DH. Neurofibromatosis type 1: a multidisciplinary approach to care.
738 Lancet Neurol. 2014;13(8):834-43. doi: 10.1016/S1474-4422(14)70063-8. PubMed PMID:
739 25030515.
740 22. Cichowski K, Jacks T. NF1 tumor suppressor gene function: narrowing the GAP. Cell.
741 2001;104(4):593-604. doi: 10.1016/s0092-8674(01)00245-8. PubMed PMID: 11239415.
742 23. Grice GL, Nathan JA. The recognition of ubiquitinated proteins by the proteasome. Cell Mol
743 Life Sci. 2016;73(18):3497-506. Epub 20160502. doi: 10.1007/s00018-016-2255-5. PubMed
744 PMID: 27137187; PMCID: PMC4980412.
745 24. Knowles TP, Vendruscolo M, Dobson CM. The amyloid state and its association with protein
746 misfolding diseases. Nat Rev Mol Cell Biol. 2014;15(6):384-96. doi: 10.1038/nrm3810.
747 PubMed PMID: 24854788.
748 25. Yakupova EI, Bobyleva LG, Vikhlyantsev IM, Bobylev AG. Congo Red and amyloids:
749 history and relationship. Biosci Rep. 2019;39(1). Epub 20190115. doi:
750 10.1042/BSR20181415. PubMed PMID: 30567726; PMCID: PMC6331669.
751 26. Kayed R, Head E, Thompson JL, McIntire TM, Milton SC, Cotman CW, Glabe CG.
752 Common structure of soluble amyloid oligomers implies common mechanism of

753 pathogenesis. Science. 2003;300(5618):486-9. doi: 10.1126/science.1079469. PubMed
754 PMID: 12702875.
755 27. Kayed R, Head E, Sarsoza F, Saing T, Cotman CW, Necula M, Margol L, Wu J, Breydo L,
756 Thompson JL, Rasool S, Gurlo T, Butler P, Glabe CG. Fibril specific, conformation
757 dependent antibodies recognize a generic epitope common to amyloid fibrils and fibrillar
758 oligomers that is absent in prefibrillar oligomers. Mol Neurodegener. 2007;2:18. Epub
759 20070926. doi: 10.1186/1750-1326-2-18. PubMed PMID: 17897471; PMCID:
760 PMC2100048.
761 28. Heiser V, Scherzinger E, Boeddrich A, Nordhoff E, Lurz R, Schugardt N, Lehrach H,
762 Wanker EE. Inhibition of huntingtin fibrillogenesis by specific antibodies and small
763 molecules: implications for Huntington's disease therapy. Proc Natl Acad Sci U S A.
764 2000;97(12):6739-44. doi: 10.1073/pnas.110138997. PubMed PMID: 10829068; PMCID:
765 PMC18723.
766 29. Sanchez I, Mahlke C, Yuan J. Pivotal role of oligomerization in expanded polyglutamine
767 neurodegenerative disorders. Nature. 2003;421(6921):373-9. doi: 10.1038/nature01301.
768 PubMed PMID: 12540902.
769 30. Tang Z, Su KH, Xu M, Dai C. HSF1 physically neutralizes amyloid oligomers to empower
770 overgrowth and bestow neuroprotection. Sci Adv. 2020;6(46). Epub 20201111. doi:
771 10.1126/sciadv.abc6871. PubMed PMID: 33177089; PMCID: PMC7673739.
772 31. Christensen JH, Nielsen MN, Hansen J, Fuchtbauer A, Fuchtbauer EM, West M, Corydon
773 TJ, Gregersen N, Bross P. Inactivation of the hereditary spastic paraplegia-associated Hspd1
774 gene encoding the Hsp60 chaperone results in early embryonic lethality in mice. Cell Stress
775 Chaperones. 2010;15(6):851-63. doi: 10.1007/s12192-010-0194-x. PubMed PMID:

776 20393889; PMCID: PMC3024079.
777 32. Fan F, Duan Y, Yang F, Trexler C, Wang H, Huang L, Li Y, Tang H, Wang G, Fang X, Liu
778 J, Jia N, Chen J, Ouyang K. Deletion of heat shock protein 60 in adult mouse cardiomyocytes
779 perturbs mitochondrial protein homeostasis and causes heart failure. Cell Death Differ.
780 2020;27(2):587-600. Epub 20190617. doi: 10.1038/s41418-019-0374-x. PubMed PMID:
781 31209364; PMCID: PMC7205885.
782 33. Su KH, Cao J, Tang Z, Dai S, He Y, Sampson SB, Benjamin IJ, Dai C. HSF1 critically
783 attunes proteotoxic stress sensing by mTORC1 to combat stress and promote growth. Nat
784 Cell Biol. 2016;18(5):527-39. Epub 20160404. doi: 10.1038/ncb3335. PubMed PMID:
785 27043084; PMCID: PMC5341796.
786 34. Johnson GL, Nakamura K. The c-jun kinase/stress-activated pathway: regulation, function
787 and role in human disease. Biochim Biophys Acta. 2007;1773(8):1341-8. Epub 20070104.
788 doi: 10.1016/j.bbamcr.2006.12.009. PubMed PMID: 17306896; PMCID: PMC1995559.
789 35. Battaglioni S, Benjamin D, Walchli M, Maier T, Hall MN. mTOR substrate phosphorylation
790 in growth control. Cell. 2022;185(11):1814-36. Epub 20220516. doi:
791 10.1016/j.cell.2022.04.013. PubMed PMID: 35580586.
792 36. Kim DH, Sarbassov DD, Ali SM, King JE, Latek RR, Erdjument-Bromage H, Tempst P,
793 Sabatini DM. mTOR interacts with raptor to form a nutrient-sensitive complex that signals to
794 the cell growth machinery. Cell. 2002;110(2):163-75. doi: 10.1016/s0092-8674(02)00808-5.
795 PubMed PMID: 12150925.
796 37. Schmidt EK, Clavarino G, Ceppi M, Pierre P. SUnSET, a nonradioactive method to monitor
797 protein synthesis. Nat Methods. 2009;6(4):275-7. Epub 20090322. doi: 10.1038/nmeth.1314.
798 PubMed PMID: 19305406.

799 38. Zhang T, Inesta-Vaquera F, Niepel M, Zhang J, Ficarro SB, Machleidt T, Xie T, Marto JA,
800 Kim N, Sim T, Laughlin JD, Park H, LoGrasso PV, Patricelli M, Nomanbhoy TK, Sorger
801 PK, Alessi DR, Gray NS. Discovery of potent and selective covalent inhibitors of JNK.
802 Chem Biol. 2012;19(1):140-54. doi: 10.1016/j.chembiol.2011.11.010. PubMed PMID:
803 22284361; PMCID: PMC3270411.
804 39. Moerke NJ, Aktas H, Chen H, Cantel S, Reibarkh MY, Fahmy A, Gross JD, Degterev A,
805 Yuan J, Chorev M, Halperin JA, Wagner G. Small-molecule inhibition of the interaction
806 between the translation initiation factors eIF4E and eIF4G. Cell. 2007;128(2):257-67. doi:
807 10.1016/j.cell.2006.11.046. PubMed PMID: 17254965.
808 40. Tolcher A, Goldman J, Patnaik A, Papadopoulos KP, Westwood P, Kelly CS, Bumgardner
809 W, Sams L, Geeganage S, Wang T, Capen AR, Huang J, Joseph S, Miller J, Benhadji KA,
810 Brail LH, Rosen LS. A phase I trial of LY2584702 tosylate, a p70 S6 kinase inhibitor, in
811 patients with advanced solid tumours. Eur J Cancer. 2014;50(5):867-75. Epub 20140115.
812 doi: 10.1016/j.ejca.2013.11.039. PubMed PMID: 24440085.
813 41. Porter AG, Janicke RU. Emerging roles of caspase-3 in apoptosis. Cell Death Differ.
814 1999;6(2):99-104. doi: 10.1038/sj.cdd.4400476. PubMed PMID: 10200555.
815 42. Boulares AH, Yakovlev AG, Ivanova V, Stoica BA, Wang G, Iyer S, Smulson M. Role of
816 poly(ADP-ribose) polymerase (PARP) cleavage in apoptosis. Caspase 3-resistant PARP
817 mutant increases rates of apoptosis in transfected cells. J Biol Chem. 1999;274(33):22932-40.
818 doi: 10.1074/jbc.274.33.22932. PubMed PMID: 10438458.
819 43. Huang J, Manning BD. The TSC1-TSC2 complex: a molecular switchboard controlling cell
820 growth. Biochem J. 2008;412(2):179-90. doi: 10.1042/BJ20080281. PubMed PMID:
821 18466115; PMCID: PMC2735030.

822 44. Dong B, Jaeger AM, Hughes PF, Loiselle DR, Hauck JS, Fu Y, Haystead TA, Huang J,
823 Thiele DJ. Targeting therapy-resistant prostate cancer via a direct inhibitor of the human heat
824 shock transcription factor 1. Sci Transl Med. 2020;12(574). doi:
825 10.1126/scitranslmed.abb5647. PubMed PMID: 33328331; PMCID: PMC10571035.
826 45. Sengupta S, Giaime E, Narayan S, Hahm S, Howell J, O'Neill D, Vlasuk GP, Saiah E.
827 Discovery of NV-5138, the first selective Brain mTORC1 activator. Sci Rep.
828 2019;9(1):4107. Epub 20190311. doi: 10.1038/s41598-019-40693-5. PubMed PMID:
829 30858438; PMCID: PMC6412019.
830 46. Kato T, Pothula S, Liu RJ, Duman CH, Terwilliger R, Vlasuk GP, Saiah E, Hahm S, Duman
831 RS. Sestrin modulator NV-5138 produces rapid antidepressant effects via direct mTORC1
832 activation. J Clin Invest. 2019;129(6):2542-54. Epub 20190416. doi: 10.1172/JCI126859.
833 PubMed PMID: 30990795; PMCID: PMC6546461.
834 47. Wolfson RL, Chantranupong L, Saxton RA, Shen K, Scaria SM, Cantor JR, Sabatini DM.
835 Sestrin2 is a leucine sensor for the mTORC1 pathway. Science. 2016;351(6268):43-8. Epub
836 20151008. doi: 10.1126/science.aab2674. PubMed PMID: 26449471; PMCID:
837 PMC4698017.
838 48. Caserta TM, Smith AN, Gultice AD, Reedy MA, Brown TL. Q-VD-OPh, a broad spectrum
839 caspase inhibitor with potent antiapoptotic properties. Apoptosis. 2003;8(4):345-52. doi:
840 10.1023/a:1024116916932. PubMed PMID: 12815277.
841 49. Chauvier D, Ankri S, Charriaut-Marlangue C, Casimir R, Jacotot E. Broad-spectrum caspase
842 inhibitors: from myth to reality? Cell Death Differ. 2007;14(2):387-91. Epub 20060929. doi:
843 10.1038/sj.cdd.4402044. PubMed PMID: 17008913.
844 50. Miao EA, Rajan JV, Aderem A. Caspase-1-induced pyroptotic cell death. Immunol Rev.

845 2011;243(1):206-14. doi: 10.1111/j.1600-065X.2011.01044.x. PubMed PMID: 21884178;
846 PMCID: PMC3609431.
847 51. Shan B, Pan H, Najafov A, Yuan J. Necroptosis in development and diseases. Genes Dev.
848 2018;32(5-6):327-40. doi: 10.1101/gad.312561.118. PubMed PMID: 29593066; PMCID:
849 PMC5900707.
850 52. Chen X, Comish PB, Tang D, Kang R. Characteristics and Biomarkers of Ferroptosis. Front
851 Cell Dev Biol. 2021;9:637162. Epub 20210121. doi: 10.3389/fcell.2021.637162. PubMed
852 PMID: 33553189; PMCID: PMC7859349.
853 53. Stockwell BR. Ferroptosis turns 10: Emerging mechanisms, physiological functions, and
854 therapeutic applications. Cell. 2022;185(14):2401-21. doi: 10.1016/j.cell.2022.06.003.
855 PubMed PMID: 35803244; PMCID: PMC9273022.
856 54. Yoshii SR, Mizushima N. Monitoring and Measuring Autophagy. Int J Mol Sci. 2017;18(9).
857 Epub 20170828. doi: 10.3390/ijms18091865. PubMed PMID: 28846632; PMCID:
858 PMC5618514.
859 55. Blommaart EF, Krause U, Schellens JP, Vreeling-Sindelarova H, Meijer AJ. The
860 phosphatidylinositol 3-kinase inhibitors wortmannin and LY294002 inhibit autophagy in
861 isolated rat hepatocytes. Eur J Biochem. 1997;243(1-2):240-6. doi: 10.1111/j.1432-
862 1033.1997.0240a.x. PubMed PMID: 9030745.
863 56. Schubert U, Anton LC, Gibbs J, Norbury CC, Yewdell JW, Bennink JR. Rapid degradation
864 of a large fraction of newly synthesized proteins by proteasomes. Nature.
865 2000;404(6779):770-4. doi: 10.1038/35008096. PubMed PMID: 10783891.
866 57. Kim LC, Cook RS, Chen J. mTORC1 and mTORC2 in cancer and the tumor
867 microenvironment. Oncogene. 2017;36(16):2191-201. Epub 20161017. doi:

868 10.1038/onc.2016.363. PubMed PMID: 27748764; PMCID: PMC5393956.
869 58. Zou Z, Tao T, Li H, Zhu X. mTOR signaling pathway and mTOR inhibitors in cancer:
870 progress and challenges. Cell Biosci. 2020;10:31. Epub 20200310. doi: 10.1186/s13578-020-
871 00396-1. PubMed PMID: 32175074; PMCID: PMC7063815.
872 59. Goloudina AR, Demidov ON, Garrido C. Inhibition of HSP70: a challenging anti-cancer
873 strategy. Cancer Lett. 2012;325(2):117-24. Epub 20120628. doi:
874 10.1016/j.canlet.2012.06.003. PubMed PMID: 22750096.
875 60. Jhaveri K, Taldone T, Modi S, Chiosis G. Advances in the clinical development of heat
876 shock protein 90 (Hsp90) inhibitors in cancers. Biochim Biophys Acta. 2012;1823(3):742-
877 55. Epub 20111029. doi: 10.1016/j.bbamcr.2011.10.008. PubMed PMID: 22062686;
878 PMCID: PMC3288123.
879 61. Pasqua AE, Sharp SY, Chessum NEA, Hayes A, Pellegrino L, Tucker MJ, Miah A, Wilding
880 B, Evans LE, Rye CS, Mok NY, Liu M, Henley AT, Gowan S, De Billy E, Te Poele R,
881 Powers M, Eccles SA, Clarke PA, Raynaud FI, Workman P, Jones K, Cheeseman MD. HSF1
882 Pathway Inhibitor Clinical Candidate (CCT361814/NXP800) Developed from a Phenotypic
883 Screen as a Potential Treatment for Refractory Ovarian Cancer and Other Malignancies. J
884 Med Chem. 2023;66(8):5907-36. Epub 20230405. doi: 10.1021/acs.jmedchem.3c00156.
885 PubMed PMID: 37017629; PMCID: PMC10150365.
886 62. Ali ES, Mitra K, Akter S, Ramproshad S, Mondal B, Khan IN, Islam MT, Sharifi-Rad J,
887 Calina D, Cho WC. Recent advances and limitations of mTOR inhibitors in the treatment of
888 cancer. Cancer Cell Int. 2022;22(1):284. Epub 20220915. doi: 10.1186/s12935-022-02706-8.
889 PubMed PMID: 36109789; PMCID: PMC9476305.
890 63. Wood KC, Gutkind JS. Challenges and Emerging Opportunities for Targeting mTOR in

891 Cancer. Cancer Res. 2022;82(21):3884-7. doi: 10.1158/0008-5472.CAN-22-0602. PubMed
892 PMID: 36321262; PMCID: PMC9634680.
893 64. Thomson AW, Turnquist HR, Raimondi G. Immunoregulatory functions of mTOR
894 inhibition. Nat Rev Immunol. 2009;9(5):324-37. doi: 10.1038/nri2546. PubMed PMID:
895 19390566; PMCID: PMC2847476.
896
897
898
899
900
901
902
903
904
905
906
907
908
909
910
911
912
913

Figure 1

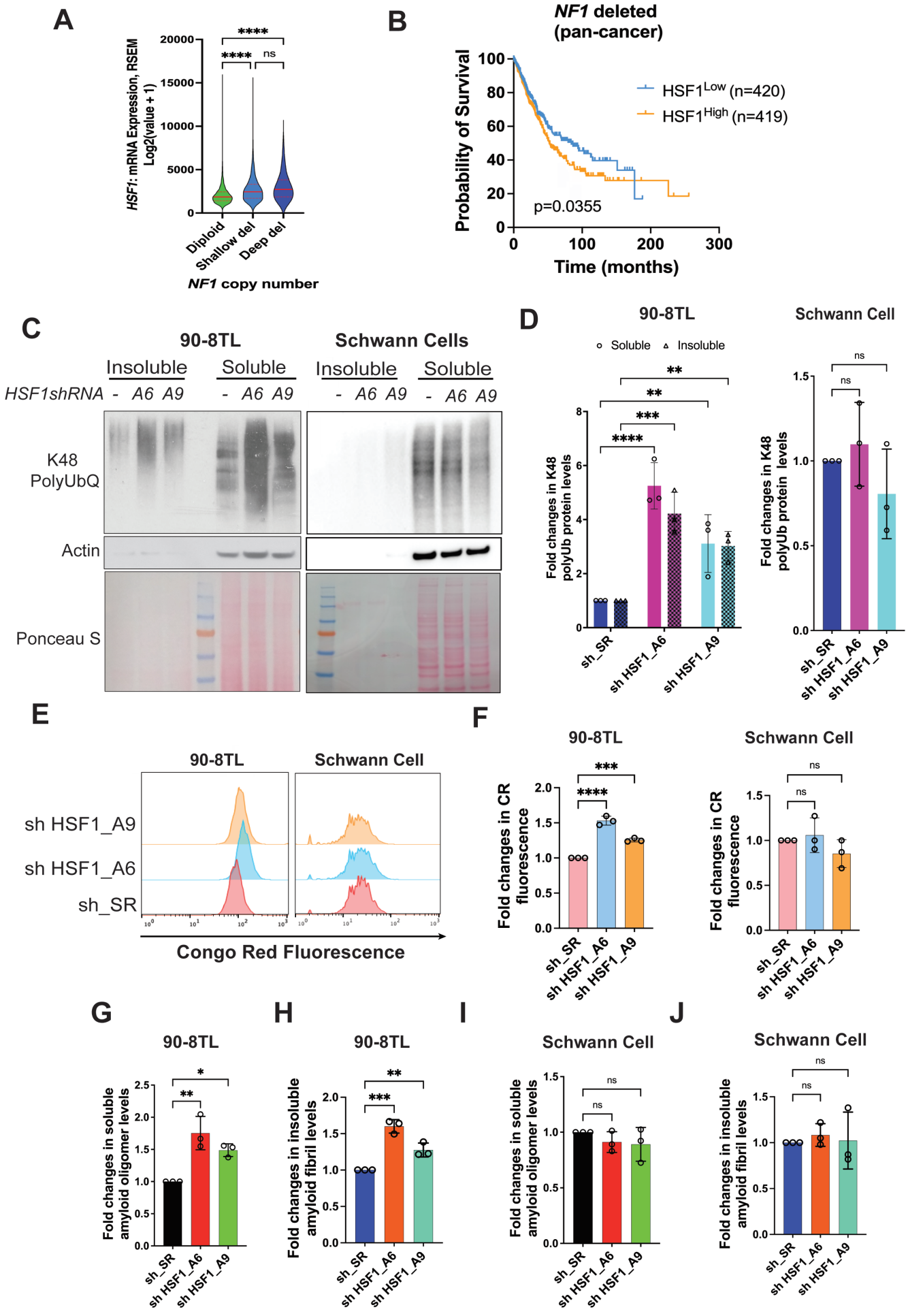
A
HSF1: mRNA Expression, RSEM Log2(value + 1)
20000
15000
10000
5000
0
****
****
ns
Diploid
Shallow del
Deep del
NF1 copy number
B
NF1 deleted (pan-cancer)
Probability of Survival
100
80
60
40
20
0
HSF1Low (n=420)
HSF1High (n=419)
p=0.0355
0
100
200
300
Time (months)
C
90-8TL
Schwann Cells
Insoluble
Soluble
Insoluble
Soluble
HSF1shRNA - A6 A9 - A6 A9 - A6 A9 - A6 A9
K48 PolyUbQ
Actin
Ponceau S
D
90-8TL
Schwann Cell
Soluble
Insoluble
Fold changes in K48 polyUb protein levels
**
**
***
****
ns
ns
sh_SR
sh HSF1_A6
sh HSF1_A9
E
90-8TL
Schwann Cell
sh HSF1_A9
sh HSF1_A6
sh_SR
Congo Red Fluorescence
F
90-8TL
Schwann Cell
Fold changes in CR fluorescence
***
****
ns
ns
sh_SR
sh HSF1_A6
sh HSF1_A9
G
90-8TL
Fold changes in soluble amyloid oligomer levels
*
**
H
90-8TL
Fold changes in insoluble amyloid fibril levels
**
***
I
Schwann Cell
Fold changes in soluble amyloid oligomer levels
ns
ns
J
Schwann Cell
Fold changes in insoluble amyloid fibril levels
ns
ns

914 **FIGURE LEGENDS:**

915 **Figure 1: HSF1 is required to suppress proteomic instability and amyloidogenesis in**
916 **MPNST cells.** (A) Violin plots of *HSF1* expression in human cancer tissues showing *NF1*
917 deletion (median and IQR, n=6424, 1598, or 88, Kruskal-Wallis test). Data are generated by the
918 TGCA Research Network (https://www.cancer.gov/tcga). (B) Kaplan-Meier survival curves of
919 patients whose tumors harbor *NF1* deletion (n=420 or 419, Log-rank test). Data are generated by
920 the TGCA Research Network (https://www.cancer.gov/tcga). (C) and (D) The impacts of *HSF1*
921 depletion on protein polyubiquitination in both 90-8TL cells and primary human Schwann cells.
922 Cells were transduced with lentiviral shRNAs for 4 days and global protein Lys48-specific
923 ubiquitination was detected by immunoblotting in both detergent-soluble and -insoluble fractions
924 of whole cell lysates (C). Protein ubiquitination was quantitated using Fiji imaging software (D)
925 (mean ± SD, n=3 independent experiments, Two-way ANOVA). (E) and (F) Congo Red (CR)
926 staining of 90-8TL cells and primary human Schwann cells with and without *HSF1* depletion,
927 analyzed by flow cytometry (E). Quantitation of CR staining using the median fluorescence
928 intensity (F) (mean ± SD, n=3 independent experiments, One-way ANOVA). (G)-(J)
929 Quantitation of soluble amyloid oligomers and insoluble amyloid fibrils by ELISA using A11
930 and OC antibodies, respectively (mean ± SD, n=3 independent experiments, One-way ANOVA).
931
932
933
934
935
936

Figure 2

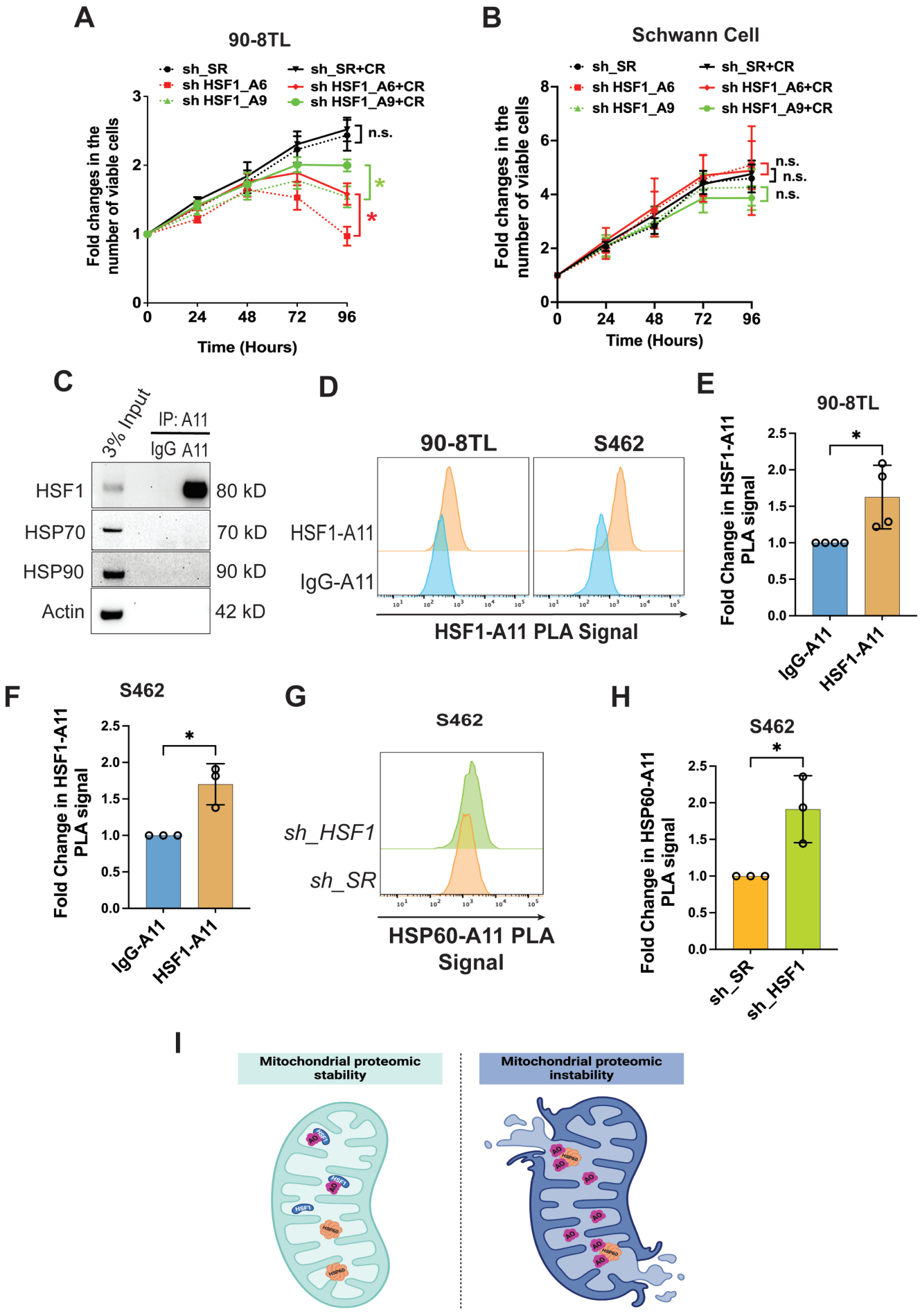
A
90-8TL
sh_SR
sh HSF1_A6
sh HSF1_A9
sh_SR+CR
sh HSF1_A6+CR
sh HSF1_A9+CR
Fold changes in the number of viable cells
Time (Hours)
n.s.
*
*
B
Schwann Cell
n.s.
n.s.
n.s.
C
3% Input
IP: A11
IgG A11
HSF1
HSP70
HSP90
Actin
80 kD
70 kD
90 kD
42 kD
D
90-8TL
S462
HSF1-A11
IgG-A11
HSF1-A11 PLA Signal
E
90-8TL
Fold Change in HSF1-A11 PLA signal
IgG-A11
HSF1-A11
F
S462
G
S462
sh_HSF1
sh_SR
HSP60-A11 PLA Signal
H
S462
Fold Change in HSP60-A11 PLA signal
sh_SR
sh_HSF1
I
Mitochondrial proteomic stability
Mitochondrial proteomic instability

937 **Figure 2: HSF1 counters the tumor-suppressive effects of amyloids in MPNST cells.**

938 (A) and (B) The growth curves of 90-8TL and primary human Schwann cells with and without

939 *HSF1* depletion and 20 μM CR treatment (mean ± SD, n=3 independent experiments, Two-way

940 ANOVA). (C) Co-IP of amyloid oligomers (AOs) with HSF1 in 90-8TL cells. (D)-(F) Detection

941 of AO-HSF1 interactions by PLA flow cytometry (D). Quantitation of AO-HSF1 PLA using the

942 median fluorescence intensity (F) (mean ± SD, n=3 or 4 independent experiments, Student's t

943 test). (G) and (H) Detection of AO-HSP60 interactions by PLA flow cytometry in S462 cells

944 following *HSF1* depletion (G). Quantitation of AO-HSP60 PLA using the median fluorescence

945 intensity (F) (mean ± SD, n=3 independent experiments, Student's t test). (I) Schematic depiction

946 of AO neuralization by HSF1 and HSP60 attack by AO following *HSF1* depletion in

947 mitochondria.

948

949

950

951

952

953

954

955

956

957

958

959

Figure 3

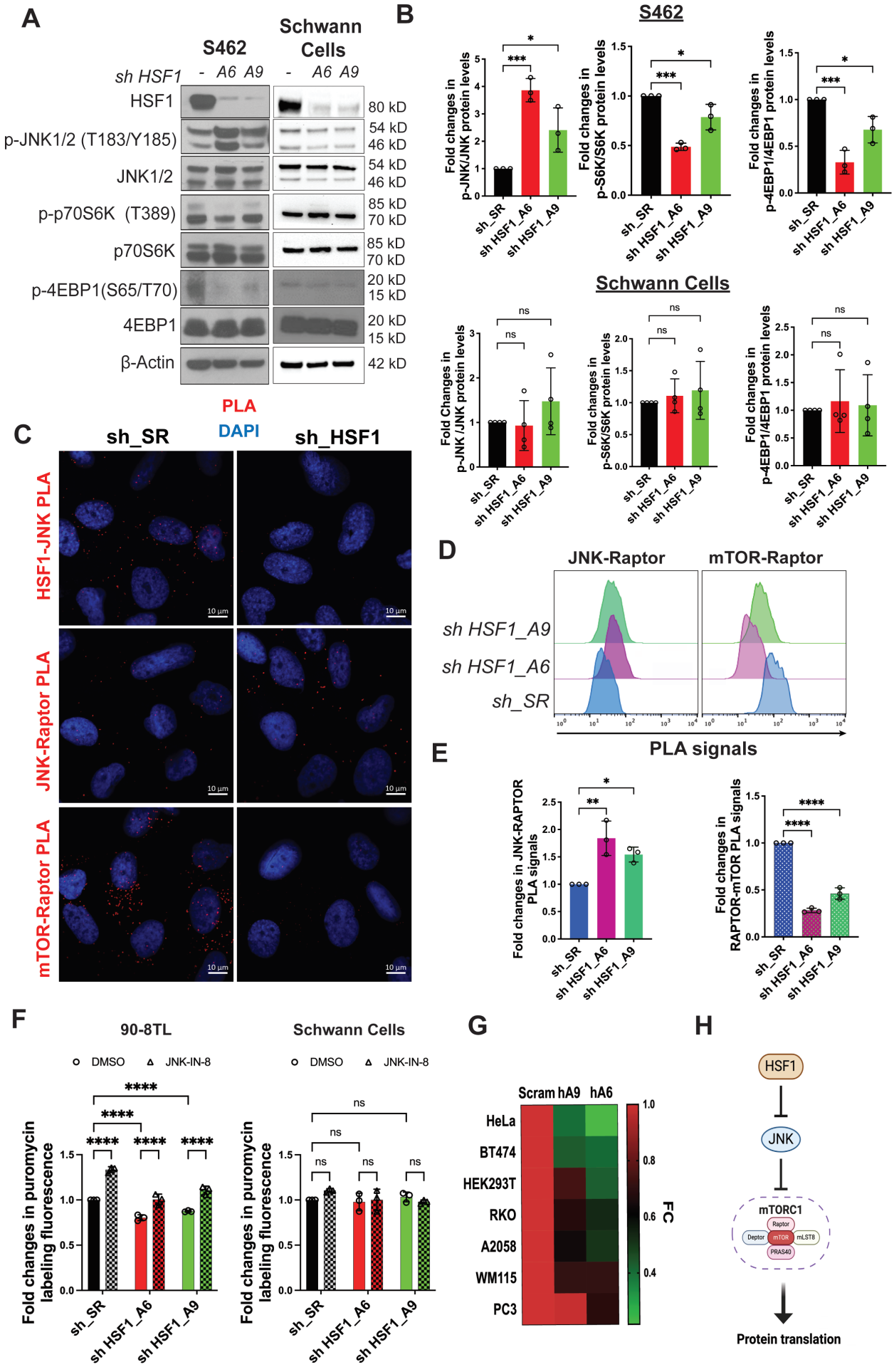
A
S462
Schwann Cells
sh HSF1
- A6 A9
- A6 A9
HSF1
p-JNK1/2 (T183/Y185)
JNK1/2
p-p70S6K (T389)
p70S6K
p-4EBP1(S65/T70)
4EBP1
β-Actin
80 kD
54 kD
46 kD
54 kD
46 kD
85 kD
70 kD
85 kD
70 kD
20 kD
15 kD
20 kD
15 kD
42 kD
B
S462
Fold changes in p-JNK/JNK protein levels
Fold changes in p-S6K/S6K protein levels
Fold changes in p-4EBP1/4EBP1 protein levels
sh_SR
sh HSF1_A6
sh HSF1_A9
Schwann Cells
Fold Changes in p-JNK /JNK protein levels
Fold changes in p-S6K/S6K protein levels
Fold changes in p-4EBP1/4EBP1 protein levels
ns
C
PLA
DAPI
sh_SR
sh_HSF1
HSF1-JNK PLA
JNK-Raptor PLA
mTOR-Raptor PLA
10 µm
D
JNK-Raptor
mTOR-Raptor
sh HSF1_A9
sh HSF1_A6
sh_SR
PLA signals
E
Fold changes in JNK-RAPTOR PLA signals
Fold changes in RAPTOR-mTOR PLA signals
sh_SR
sh HSF1_A6
sh HSF1_A9
F
90-8TL
Schwann Cells
DMSO
JNK-IN-8
Fold changes in puromycin labeling fluorescence
sh_SR
sh HSF1_A6
sh HSF1_A9
G
Scram hA9 hA6
HeLa
BT474
HEK293T
RKO
A2058
WM115
PC3
FC
H
HSF1
JNK
mTORC1
Raptor
Deptor
mTOR
mLST8
PRAS40
Protein translation

960 **Figure 3: JNK senses *HSF1* deficiency to repress mTORC1 and protein translation in**
961 **MPNST cells.** (A) Detection of JNK activation and mTORC1 inhibition following *HSF1*
962 depletion in S462 and primary human Schwann cells by immunoblotting. (B) Quantitation of (A)
963 using Fiji imaging software (mean ± SD, n=3 independent experiments, One-way ANOVA). (C)
964 Detection of HSF1-JNK, JNK-RAPTOR, and mTOR-RAPTOR interactions by PLA in S462
965 cells with and without *HSF1* depletion. (D) and (E) Detection and quantitation of JNK-RAPTOR
966 and mTOR-RAPTOR interactions by PLA flow cytometry in 90-8TL cells (mean ± SD, n=3
967 independent experiments, One-way ANOVA). (F) Measurement of protein translation rates in
968 90-8TL and primary human Schwann cells with and without *HSF1* depletion by puromycin
969 labeling, analyzed by flow cytometry. Cells were treated with 1 μM JNK-IN-8 for 24 hrs before
970 labeling with 100 nM 6-FAM-dc-puromycin for 30 min (mean ± SD, n=3 independent
971 experiments, Two-way ANOVA). (G) Heatmap of protein translation rates measured by
972 puromycin labeling in diverse human cancer cell lines with and without *HSF1* depletion. (H)
973 Schematic depiction of regulation of protein translation by HSF1.
974
975
976
977
978
979
980
981
982

Figure 4

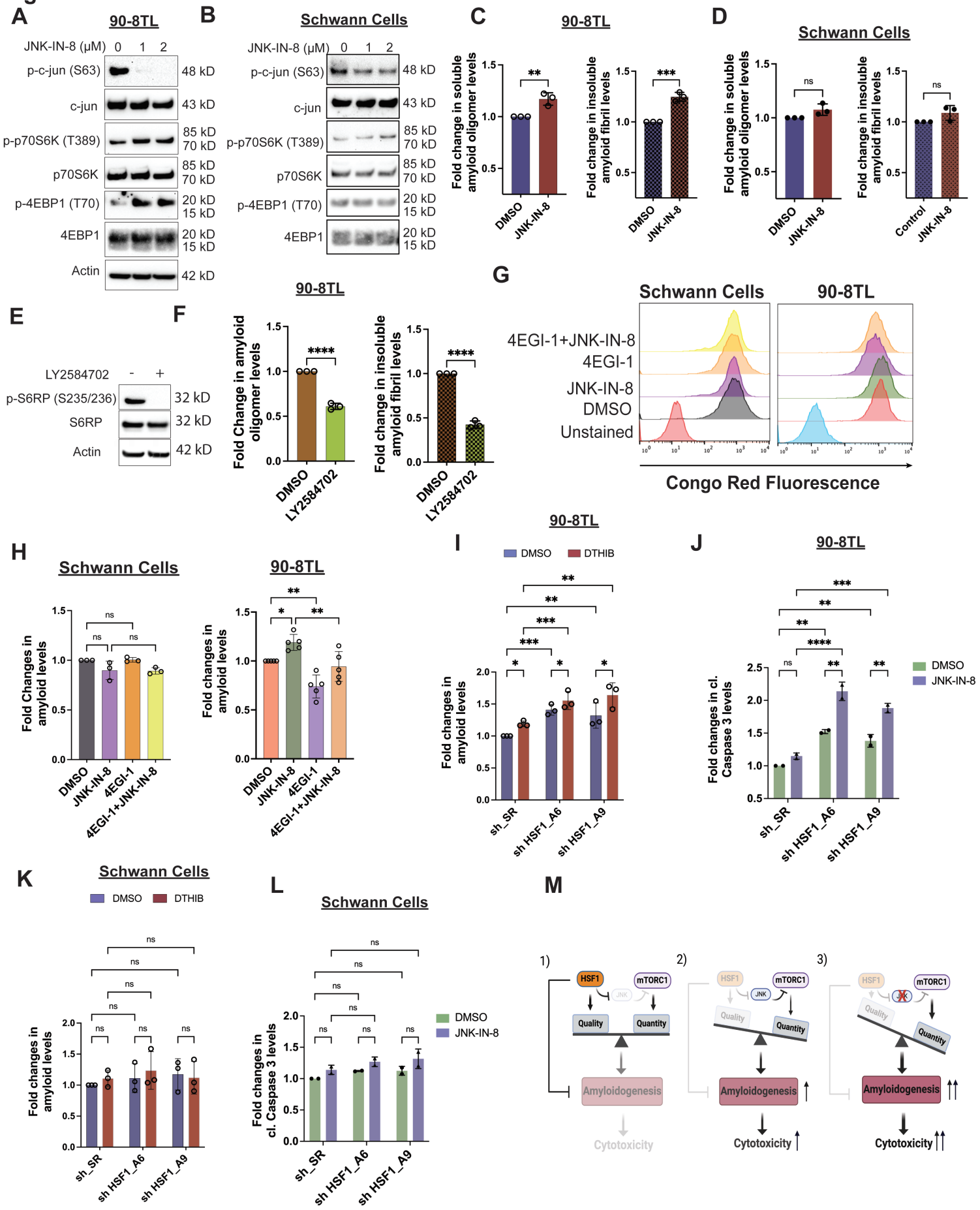
A
90-8TL
JNK-IN-8 (μM) 0 1 2
p-c-jun (S63) 48 kD
c-jun 43 kD
p-p70S6K (T389) 85 kD 70 kD
p70S6K 85 kD 70 kD
p-4EBP1 (T70) 20 kD 15 kD
4EBP1 20 kD 15 kD
Actin 42 kD
B
Schwann Cells
JNK-IN-8 (μM) 0 1 2
p-c-jun (S63) 48 kD
c-jun 43 kD
p-p70S6K (T389) 85 kD 70 kD
p70S6K 85 kD 70 kD
p-4EBP1 (T70) 20 kD 15 kD
4EBP1 20 kD 15 kD
C
90-8TL
Fold change in soluble amyloid oligomer levels
Fold change in insoluble amyloid fibril levels
DMSO
JNK-IN-8
D
Schwann Cells
Control
E
LY2584702 - +
p-S6RP (S235/236) 32 kD
S6RP 32 kD
Actin 42 kD
F
90-8TL
Fold Change in amyloid oligomer levels
Fold change in insoluble amyloid fibril levels
LY2584702
G
Schwann Cells
90-8TL
4EGI-1+JNK-IN-8
4EGI-1
JNK-IN-8
DMSO
Unstained
Congo Red Fluorescence
H
Schwann Cells
90-8TL
Fold Changes in amyloid levels
4EGI-1
4EGI-1+JNK-IN-8
I
90-8TL
DMSO
DTHIB
Fold changes in amyloid levels
sh_SR
sh HSF1_A6
sh HSF1_A9
J
90-8TL
Fold changes in cl. Caspase 3 levels
K
Schwann Cells
L
Schwann Cells
M
1)
2)
3)
HSF1
mTORC1
JNK
Quality
Quantity
Amyloidogenesis
Cytotoxicity

983 **Figure 4: Protein translation is causally related to amyloidogenesis in MPNST cells.**
984 (A) and (B) Detection of mTORC1 stimulation following JNK inhibition in 90-8TL and
985 immortalized human Schwann cells by immunoblotting. Cells were treated with JNK-IN-8 for 2
986 days. (C) and (D) Quantitation of soluble AOs and insoluble AFs by ELISA in 90-8TL and
987 human Schwann cells with and without 3 μM JNK-IN-8 treatment for 3 days (mean ± SD, n=3
988 independent experiments, Student's t test). (E) Detection of LY2584702-mediated S6K
989 inhibition in 90-8TL cells by immunoblotting. Cells were treated with 20 μM LY2584702 for 2
990 days. (F) Quantitation of soluble AOs and insoluble AFs by ELISA in 90-8TL cells with and
991 without 20 μM LY2584702 treatment for 2 days (mean ± SD, n=3 independent experiments,
992 Student's t test). (G) CR staining of 90-8TL and immortalized human Schwann cells with and
993 without JNK-IN-8 and 4EGI-1 treatment, detected by flow cytometry. (H) Quantitation of (G)
994 using the median fluorescence intensity (mean ± SD, n=3 independent experiments, One-way
995 ANOVA). (I) Quantitation of amyloids by CR staining in 90-8TL cells with and without *HSF1*
996 depletion and 3 μM JNK-IN-8 treatment (mean ± SD, n=3 independent experiments, Two-way
997 ANOVA). (J) Quantitation of caspase 3 cleavage by ELISA in 90-8TL cells with and without
998 *HSF1* depletion and 3 μM JNK-IN-8 treatment (mean ± SD, n=2 independent experiments, Two-
999 way ANOVA). (K) Quantitation of amyloids by CR staining in immortalized human Schwann
1000 cells with and without *HSF1* depletion and 3 μM JNK-IN-8 treatment (mean ± SD, n=3
1001 independent experiments, Two-way ANOVA). (L) Quantitation of caspase 3 cleavage by ELISA
1002 in immortalized human Schwann cells with and without *HSF1* depletion and 3 μM JNK-IN-8
1003 treatment (mean ± SD, n=2 independent experiments, Two-way ANOVA). (M) Schematic
1004 depiction of the adaptation of MPNST cells to *HSF1* depletion by activating JNK to suppress
1005 mTORC1 and protein translation, thereby alleviating amyloidogenesis and cytotoxicity.

Figure 5

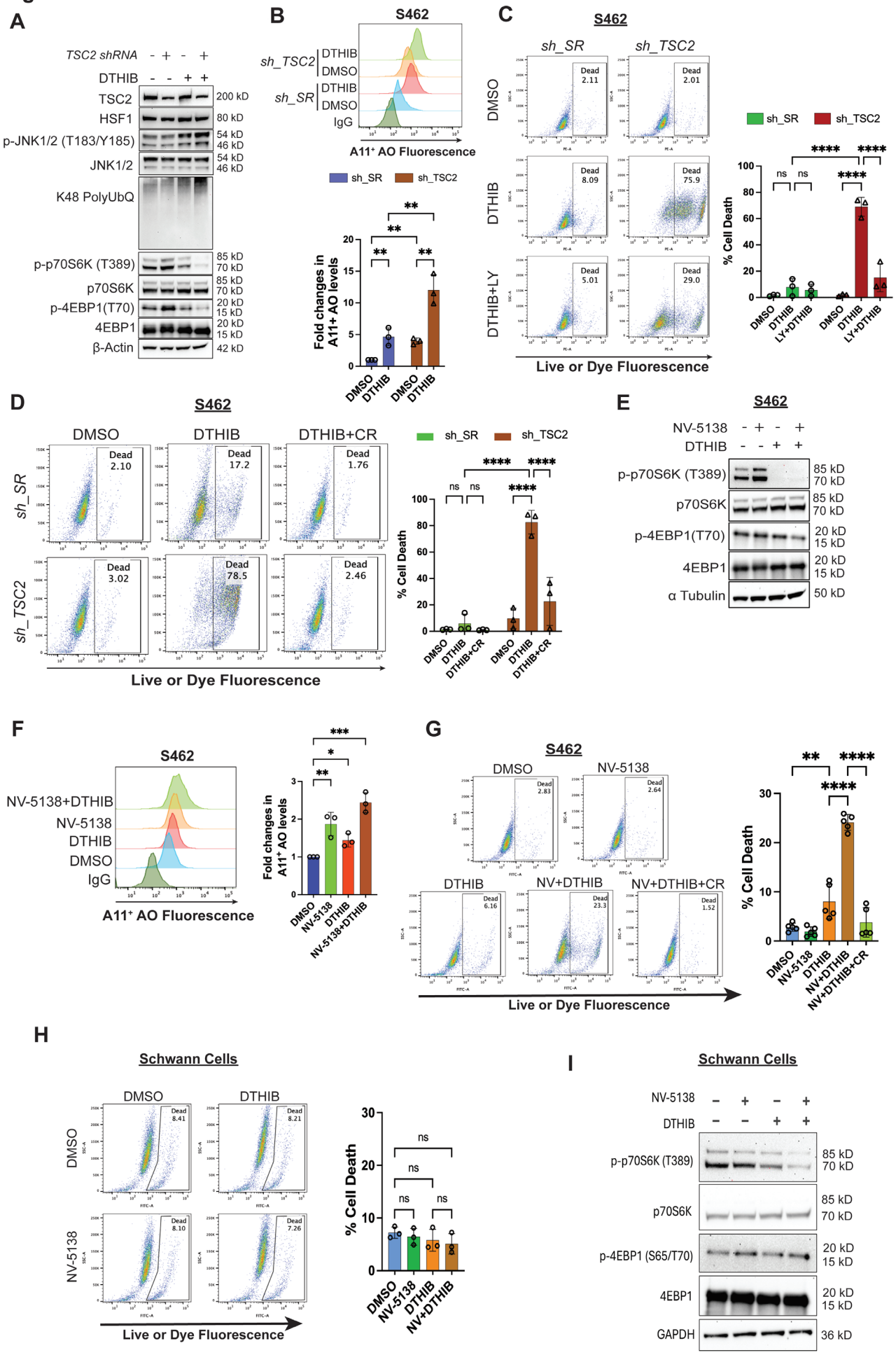
A
TSC2 shRNA - + - +
DTHIB - - + +
TSC2
HSF1
p-JNK1/2 (T183/Y185)
JNK1/2
K48 PolyUbQ
p-p70S6K (T389)
p70S6K
p-4EBP1(T70)
4EBP1
β-Actin
200 kD
80 kD
54 kD
46 kD
85 kD
70 kD
20 kD
15 kD
42 kD
B
S462
sh_TSC2
sh_SR
DTHIB
DMSO
IgG
A11+ AO Fluorescence
sh_SR
sh_TSC2
Fold changes in A11+ AO levels
DMSO
DTHIB
C
S462
sh_SR
sh_TSC2
DMSO
DTHIB
DTHIB+LY
Dead 2.11
Dead 2.01
Dead 8.09
Dead 75.9
Dead 5.01
Dead 29.0
Live or Dye Fluorescence
% Cell Death
LY+DTHIB
D
S462
DMSO
DTHIB
DTHIB+CR
Dead 2.10
Dead 17.2
Dead 1.76
Dead 3.02
Dead 78.5
Dead 2.46
Live or Dye Fluorescence
% Cell Death
E
S462
NV-5138 - + - +
DTHIB - - + +
p-p70S6K (T389)
p70S6K
p-4EBP1(T70)
4EBP1
α Tubulin
F
S462
NV-5138+DTHIB
NV-5138
DTHIB
DMSO
IgG
A11+ AO Fluorescence
Fold changes in A11+ AO levels
G
S462
DMSO
NV-5138
DTHIB
NV+DTHIB
NV+DTHIB+CR
Dead 2.83
Dead 2.64
Dead 6.16
Dead 23.3
Dead 1.52
Live or Dye Fluorescence
% Cell Death
H
Schwann Cells
DMSO
DTHIB
NV-5138
Dead 8.41
Dead 8.21
Dead 8.10
Dead 7.26
Live or Dye Fluorescence
% Cell Death
I
Schwann Cells
NV-5138 - + - +
DTHIB - - + +
p-p70S6K (T389)
p70S6K
p-4EBP1 (S65/T70)
4EBP1
GAPDH
36 kD

1006 **Figure 5: mTORC1 stimulation aggravates the amyloidogenesis and cytotoxicity elicited by**
1007 **HSF1 inhibition.** (A) Immunoblotting detection of JNK activation, mTORC1 activity, and
1008 protein polyubiquitination in S462 cells following stable *TSC2* knockdown and/or HSF1
1009 inhibition by 10 μM DTHIB for 3 days. (B) Quantitation of soluble AOs by flow cytometry
1010 using A11 antibody staining in S462 cells with and without *TSC2* knockdown and 10 μM
1011 DTHIB treatment (mean ± SD, n=3 independent experiments, Two-way ANOVA). (C)
1012 Quantitation of cytotoxicity by flow cytometry using Live-or-Dye stains in S462 cells with and
1013 without stable *TSC2* knockdown and DTHIB (10 μM) or combined DTHIB and LY2584702 (20
1014 μM) treatment (mean ± SD, n=3 independent experiments, Two-way ANOVA). Cells were pre-
1015 treated with LY2584702 for 1 day followed by DTHIB treatment for another 3 days. (D)
1016 Quantitation of cytotoxicity by flow cytometry using Live-or-Dye stains in S462 cells with and
1017 without stable *TSC2* knockdown and DTHIB (10 μM) or combined DTHIB and CR (30 μM)
1018 treatment (mean ± SD, n=3 independent experiments, Two-way ANOVA). Cells were pre-
1019 treated with CR for 1 day followed by DTHIB treatment for another 3 days. (E) Immunoblotting
1020 detection of mTORC1 stimulation by 500 μM NV-5138 in S462 cells with and without 10 μM
1021 DTHIB treatment. (F) Quantitation of soluble AOs by flow cytometry using A11 antibody
1022 staining in S462 cells with and without 500 μM NV-5138 stimulation and 10 μM DTHIB
1023 treatment (mean ± SD, n=3 independent experiments, One-way ANOVA). (G) Quantitation of
1024 cytotoxicity by flow cytometry using Live-or-Dye stains in S462 cells with and without 500 μM
1025 NV-5138 stimulation and 10 μM DTHIB or combined DTHIB and CR treatment (mean ± SD,
1026 n=5 independent experiments, One-way ANOVA). (H) Quantitation of cytotoxicity by flow
1027 cytometry using Live-or-Dye stains in immortalized human Schwann cells with and without 500
1028 μM NV-5138 stimulation and 10 μM DTHIB treatment (mean ± SD, n=3 independent

1029 experiments, One-way ANOVA). (I) Immunoblotting detection of mTORC1 stimulation by 500

1030 μM NV-5138 in immortalized human Schwann cells with and without 10 μM DTHIB treatment.

1031

1032

1033

1034

1035

1036

1037

1038

1039

1040

1041

1042

1043

1044

1045

1046

1047

1048

1049

1050

Figure 6

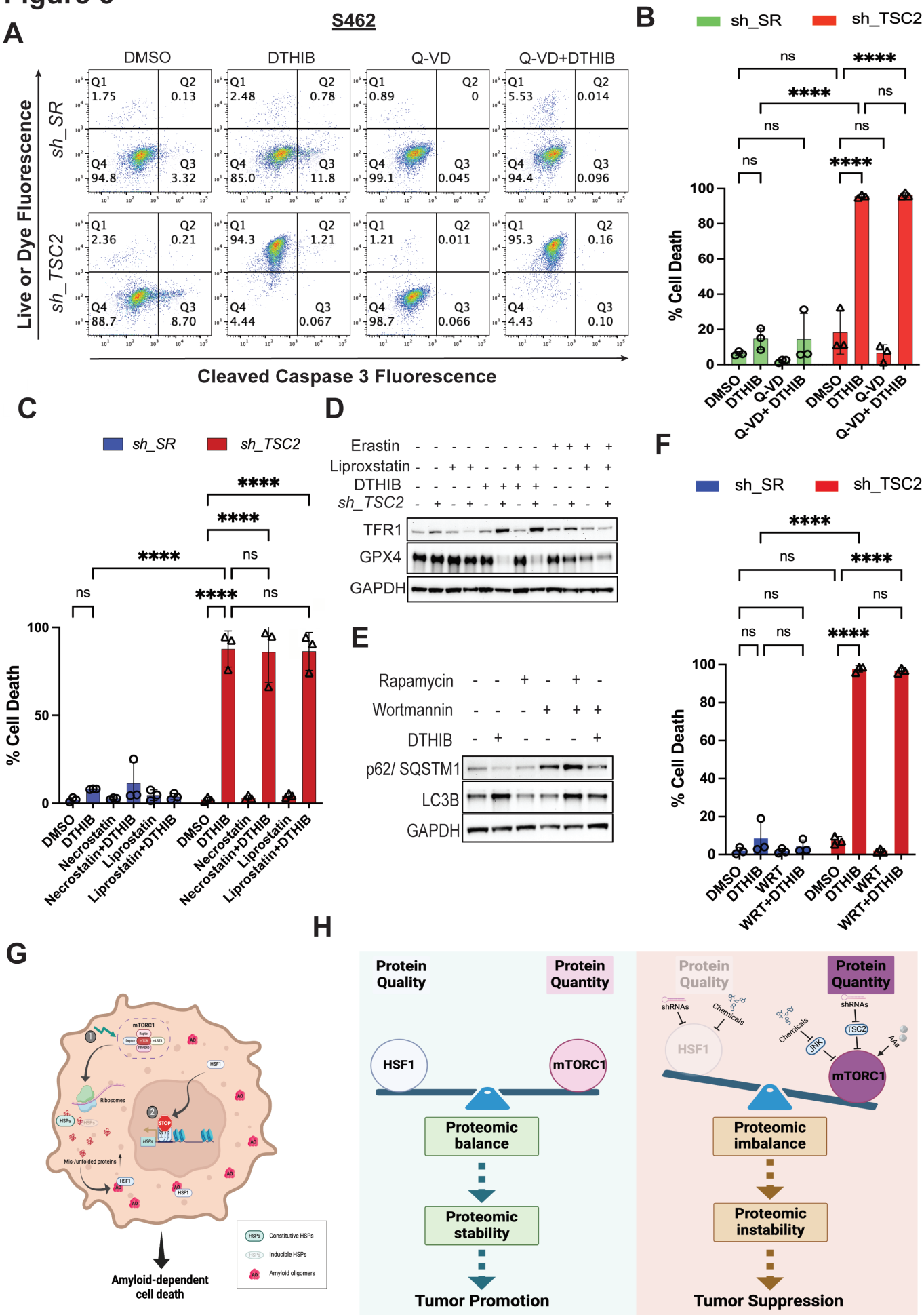

A
S462
DMSO
DTHIB
Q-VD
Q-VD+DTHIB
sh_SR
sh_TSC2
Live or Dye Fluorescence
Cleaved Caspase 3 Fluorescence
Q1 1.75
Q2 0.13
Q4 94.8
Q3 3.32
Q1 2.48
Q2 0.78
Q4 85.0
Q3 11.8
Q1 0.89
Q2 0
Q4 99.1
Q3 0.045
Q1 5.53
Q2 0.014
Q4 94.4
Q3 0.096
Q1 2.36
Q2 0.21
Q4 88.7
Q3 8.70
Q1 94.3
Q2 1.21
Q4 4.44
Q3 0.067
Q1 1.21
Q2 0.011
Q4 98.7
Q3 0.066
Q1 95.3
Q2 0.16
Q4 4.43
Q3 0.10
B
sh_SR
sh_TSC2
% Cell Death
DMSO
DTHIB
Q-VD
Q-VD+ DTHIB
C
sh_SR
sh_TSC2
% Cell Death
DMSO
DTHIB
Necrostatin
Necrostatin+DTHIB
Liprostatin
Liprostatin+DTHIB
D
Erastin
Liproxstatin
DTHIB
sh_TSC2
TFR1
GPX4
GAPDH
E
Rapamycin
Wortmannin
DTHIB
p62/ SQSTM1
LC3B
GAPDH
F
sh_SR
sh_TSC2
% Cell Death
DMSO
DTHIB
WRT
WRT+DTHIB
G
mTORC1
Ribosomes
Mis-/unfolded proteins
Amyloid-dependent cell death
Constitutive HSPs
Inducible HSPs
Amyloid oligomers
H
Protein Quality
Protein Quantity
HSF1
mTORC1
Proteomic balance
Proteomic stability
Tumor Promotion
shRNAs
Chemicals
TSC2
JNK
AAs
Proteomic imbalance
Proteomic instability
Tumor Suppression

1051 **Figure 6: Concurrent HSF1 inhibition and mTORC1 stimulation instigate widespread non-**
1052 **apoptotic cell death.** (A) and (B) Quantitation of cytotoxicity by flow cytometry using Live-or-
1053 Dye stains combined with cleaved caspase 3 (Asp175) antibody staining. S462 cells with and
1054 without stable *TSC2* knockdown were treated with DMSO, 10 μM DTHIB, or combined DTHIB
1055 and 30 μM Q-VD-OPh (mean ± SD, n=3 independent experiments, Two-way ANOVA). (C)
1056 Quantitation of cytotoxicity by flow cytometry using Live-or-Dye stains in S462 cells with and
1057 without stable *TSC2* knockdown. Cells were treated with 10 μM DTHIB alone or co-treated with
1058 10 μM DTHIB and 30 μM Necrostatin-1 or 20 μM Liproxstatin-1 for 3 days (mean ± SD, n=3
1059 independent experiments, Two-way ANOVA). (D) Immunoblotting detection of ferroptosis
1060 markers in S462 cells with and without stable *TSC2* knockdown treated with 10 μM DTHIB
1061 alone or co-treated with 10 μM DTHIB and 20 μM liproxstatin-1 for 3 days. Erastin was
1062 included as a positive control to induce canonical ferroptosis. (E) Immunoblotting detection of
1063 autophagy markers in S462 cells with stable *TSC2* knockdown treated with 10 μM DTHIB alone
1064 or co-treated with 10 μM DTHIB and 3 μM wortmannin for 3 days. Rapamycin was included as
1065 a positive control to induce autophagy. (F) Quantitation of cytotoxicity by flow cytometry using
1066 Live-or-Dye stains in S462 cells with and without stable *TSC2* knockdown. Cells were treated
1067 with 10 μM DTHIB alone or co-treated with 10 μM DTHIB and 3 μM wortmannin for 3 days
1068 (mean ± SD, n=3 independent experiments, Two-way ANOVA). (G) Schematic depiction of
1069 instigation of cell death by severe proteomic imbalance, owing to simultaneous mTORC1
1070 stimulation (❶) and HSF1 inhibition (❷). In cancer cells, constitutive HSF1 activation
1071 provides extra chaperoning capacity to cope with elevated protein misfolding, partly due to
1072 enhanced protein synthesis and widespread genetic mutations. Nevertheless, amyloids still
1073 emerge, although at low levels. Importantly, HSF1 can neutralize highly toxic amyloid

1074 oligomers, averting lethal consequences. By contrast, HSF1 inhibition diminishes chaperoning
1075 capacity, insufficient to counterbalance the robust protein translation. mTORC1 stimulation
1076 further aggravates this proteomic imbalance, which, in turn, strongly promotes amyloidogenesis.
1077 In consequence, the amounts of amyloid oligomers exceed the neutralizing capacity of HSF1,
1078 leading to cell death; nonetheless, it remains unclear how this non-apoptotic, non-autophagic
1079 death occurs. (H) Schematic depiction of the concept of driving proteomic imbalance to combat
1080 malignancy. On the one hand, in cancer cells, mTORC1 is inevitably activated to stimulate
1081 protein translation, markedly augmenting protein quantity. On the other hand, the extra
1082 chaperoning capacity governed by HSF1, albeit dispensable for normal life, becomes necessary
1083 to ensure sufficient protein quality in cancer cells, thereby counterbalancing augmented protein
1084 quantity and suppressing proteomic instability. Thus, proteomic balance promotes malignant
1085 growth. By contrast, disrupting proteomic balance, through HSF1 inhibition, is sufficient to
1086 provoke proteomic instability and elicit tumor suppression. However, simultaneous mTORC1
1087 stimulation can remarkably drive proteomic imbalance, causing severe proteomic instability and
1088 profound tumor suppression.
1089
1090
1091
1092
1093
1094
1095